© 2021. Published by The Company of Biologists Ltd | Journal of Cell Science (2021) 134, jcs259156. doi:10.1242/jcs.259156

RESEARCH ARTICLE

The mRNA decapping complex is buffered by nuclear localization

Kiril Tishinov and Anne Spang*

ABSTRACT

mRNA decay is a key step in regulating the cellular proteome. Processing bodies (P-bodies) are thought to be sites of mRNA decay and/or storage. P-body units assemble into P-body granules under stress conditions. How this assembly is regulated, however, remains poorly understood. Here, we show, in the yeast *Saccharomyces cerevisiae*, that the translational repressor Scd6 and the decapping stimulator Edc3 act partially redundantly in P-body assembly by sequestering the Dcp1–Dcp2 (denoted Dcp1/2) decapping complex in the cytoplasm and preventing it from becoming imported into the nucleus by the karyopherin β protein Kap95. One of two nuclear localization signals in Dcp2 overlaps with the RNA-binding site, suggesting an additional mechanism to regulate Dcp1/2 localization. Nuclear Dcp1/2 does not drive mRNA decay and might be stored there as a readily releasable pool, indicating a dynamic equilibrium between cytoplasmic and nuclear Dcp1/2. Cytoplasmic Dcp1/2 is linked to Dhh1 via Edc3. Functional P-bodies are present at the endoplasmic reticulum where Dcp2 potentially acts to increase the local concentration of Dhh1 through interaction with Edc3 to drive phase separation and hence P-body formation.

KEY WORDS: mRNA, Nucleo-cytoplasmic transport, Processing bodies, Membraneless granules, Phase separation, Endoplasmic reticulum

INTRODUCTION

Translational attenuation is among the first lines of defense when a cell encounters stress. Ribosomes will release mRNA, and most of the mRNA is captured into processing bodies (P-bodies), which form very quickly, within 5 min after stress encounter. The fast formation of P-bodies might be explained by the notion that the release of mRNAs and their capture into P-bodies is coordinated in two ways. First, a subset of P-body components, such as the 5′ exonuclease Xrn1, is associated with polysomes and, second, regulators of translation such as Scp160 and Bfr1 negatively regulate P-body formation (Weidner et al., 2014; Tesina et al., 2019). Moreover, P-bodies contain the translational repressor Scd6, which can sequester eIF4G (Nissan et al., 2010; Rajyaguru et al., 2012). P-bodies were initially thought to represent an mRNA decay compartment (Sheth and Parker, 2003). This decay requires removal of the 5′ 7-methylguanylate (5′ 7-mG) cap by the decapping complex Dcp1–Dcp2 (denoted Dcp1/2) . The decapping activity is stimulated by the DEAD box helicase Dhh1 (known as DDX6 in vertebrates) and the RNA-binding protein Pat1 (Nissan et al., 2010). Recent data, however, provide evidence that P-bodies do not only act as decay compartments but are also mRNA storage organelles and that the fate of an mRNA in P-bodies is dependent of the type of stressor (Wang et al., 2018; Luo et al., 2020). Not only is the fate of mRNAs in P-bodies stress dependent, but the morphology of P-bodies can also vary according to the stress. For example, under glucose starvation, one or two large P-bodies are usually observed, while hyperosmotic stress and defects in the secretory pathway induce numerous smaller P-bodies (Kilchert et al., 2010). The different morphologies also suggest that the protein composition of the P-bodies might be dependent on the stressor. Although most of the research on P-bodies has been performed in *Saccharomyces cerevisiae*, because of the evolutionary conservation of the P-body components (Fig. 1A) and its functions, the results obtained in yeast are highly relevant for all metazoans.

P-bodies are membraneless organelles. Some of the protein components contain unstructured regions or a RecA fold that are able, together with RNA, to engage in liquid–liquid phase separation. Indeed, recently it was shown that Dhh1/DDX6 could drive phase separation *in vitro* and *in vivo* (Hondele et al., 2019). Other proteins, such Pat1, Edc3 and Scd6 have also been shown to contribute to P-body assembly under at least some stress conditions (Decker et al., 2007; Teixeira and Parker, 2007; Kilchert et al., 2010; Sachdev et al., 2019). It appears as if Dhh1 and Pat1 act together, while Scd6 and Edc3 seem to have partially redundant functions in P-body formation (Coller and Parker, 2005; Decourty et al., 2008; Nissan et al., 2010). Thus, P-body assembly and function might be regulated through different pathways, consistent with the findings that a variety of kinases can regulate granule assembly (Yoon et al., 2010; Ramachandran et al., 2011). While under stress P-body are easily detected by light microscopy, they are essentially undetectable in unstressed cells. Yet, smaller P-body degradative units exist in unstressed cells as the major RNA degradation pathway in yeast is Xrn1-dependent, which acts in P-bodies (Parker, 2012). While the pathway by which Dhh1/DDX6 and Pat1 drive P-body formation is relatively well understood, information about the Scd6- and Edc3-dependent pathway is still scarce.

Therefore, we decided to analyze the role of Scd6 and Edc3 in P-body assembly. We found that both proteins are required to retain the decapping complex in the cytoplasm. In an *edc3*Δ *scd6*Δ mutant, Dcp1 and Dcp2 accumulated in the nucleus through active import by Kap95. Dcp2 appears to have two nuclear localization signals (NLSs), one of which is in the RNA-binding site, suggesting that this site would only be revealed if Dcp2 is not bound to RNA. Nuclear localized Dcp1 and Dcp2, however, did not drive nuclear mRNA decay. We propose that the nuclear decapping complex acts as a reservoir to regulate mRNA decay and decapping activity in the cytoplasm. We show furthermore that P-body assembly happens primarily on the endoplasmic reticulum (ER) and that, in this process, Edc3 links the decapping complex to Dhh1 (Fig. 1B). Taken together, we provide a novel mechanism on how cytoplasmic functional decapping complex concentration is regulated.

Biozentrum, University of Basel, Spitalstrasse 41, CH-4056 Basel, Switzerland.

*Author for correspondence (anne.spang@unibas.ch)

K.T., 0000-0003-3211-1824; A.S., 0000-0002-2387-6203

Handling Editor: Maria Carmo-Fonseca
Received 15 July 2021; Accepted 17 August 2021

Journal of Cell Science

Journal of Cell Science (2021) 134, jcs259156. doi:10.1242/jcs.259156

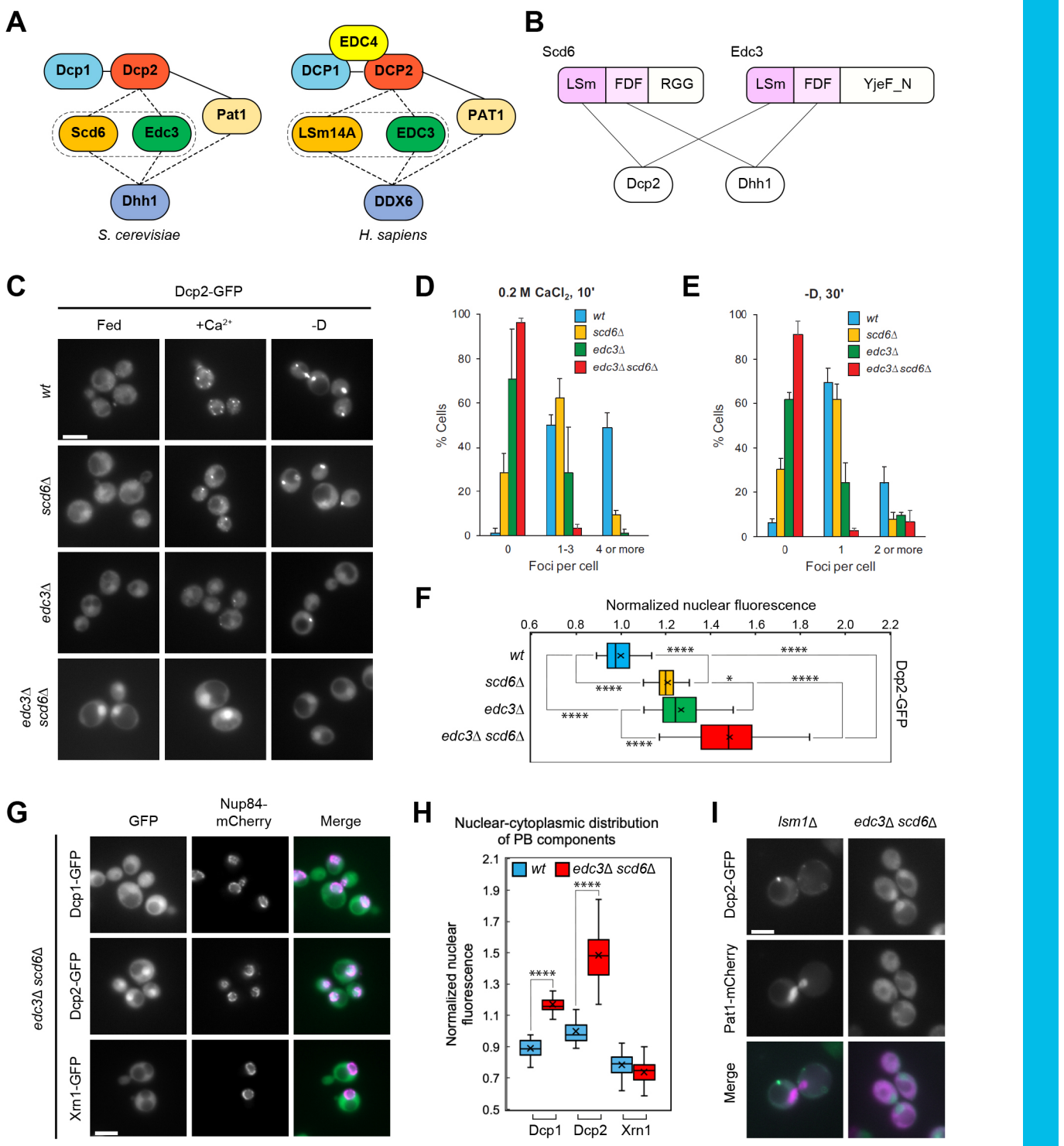

Fig. 1. See next page for legend.

RESULTS

Concomitant loss of Scd6 and Edc3 blocks P-body assembly and drives nuclear accumulation of Dcp2

Previous studies have shown that the individual deletions of *EDC3* and *SCD6* only partially affect P-body formation (Decker et al., 2007; Kilchert et al., 2010; Rajyaguru et al., 2012) and that they are dispensable for growth (Kshirsagar and Parker, 2004; Decourty et al., 2008). However, since they might have partially overlapping functions, we generated an *edc3*Δ *scd6*Δ double mutant and assessed its ability to form P-bodies under stress using Dcp2–GFP as a marker (Fig. 1C). As observed previously, deletion of either *SCD6* or *EDC3* affected P-body formation under hypoosmotic stress and to a somewhat lesser extent under starvation (Fig. 1C–E; Kilchert et al., 2010). This effect was strongly exacerbated in the double mutant, consistent with the notion of these two proteins having a redundant function in P-body granule formation.

Surprisingly, we also observed an accumulation of Dcp2–GFP in the nucleus in the single mutants, which was again strongly

Journal of Cell Science (2021) 134, jcs259156. doi:10.1242/jcs.259156

Fig. 1. Concomitant loss of Scd6 and Edc3 blocks P-body assembly and drives nuclear accumulation of Dcp2. (A) Schematic representation of the evolutionarily conserved basic P-body-components in budding yeast and humans. Dashed lines indicate mutually exclusive interactions. (B) Both Scd6 and Edc3 ensure interaction between Dcp2 and Dhh1 through common structural motifs. (C) Loss of function of *SCD6* and *EDC3* leads to defects in P-body formation under stress and nuclear enrichment of Dcp2. Logarithmically growing cells expressing genomically tagged Dcp2–GFP were imaged either directly or first shifted to the respective stress conditions [0.2 M $CaCl_2$ for 10 min (+Ca^{2+}) or glucose deprivation for 30 min (-D)]. *wt*, wild type. Scale bar: 5 µm. (D,E) Quantification of the mean±s.d. number of GFP foci from the data as shown in C from at least three independent experiments. (F) Quantification of the nuclear-cytoplasmic Dcp2–GFP distribution from the data as shown in C from at least three independent experiments. The mean nuclear GFP fluorescence of a small area of the cell nucleus was normalized to the mean GFP fluorescence of small area of the cytoplasm of the same cell. (G) In *edc3*Δ *scd6*Δ cells, the decapping complex components Dcp1 and Dcp2 are enriched in the cell nucleus while the exonuclease Xrn1 is not. Logarithmically growing *edc3*Δ *scd6*Δ cells expressing genomically tagged Dcp1–, Dcp2– or Xrn1–GFP and the nuclear marker Nup84–mCherry were imaged without additional treatment. Scale bar: 5 µm. (H) Quantification of the nuclear-cytoplasmic distribution of the GFP-tagged proteins from the data as shown in G. (I) Dcp2 and Pat1 are imported into the cell nucleus through different mechanisms. Logarithmically growing cells expressing Dcp2-GFP from a genomic locus and Pat1–mCherry from a low-copy plasmid on its own promoter were imaged without additional treatment. Images representative of three experiments. Box plots in F and H are presented as described in the Materials and Methods. **P*<0.05; *****P*<0.0001 (non-parametric test). Scale bar: 5 µm.

increased in the double mutant under normal growth conditions (Fig. 1C,F). In fact, in *edc3*Δ *scd6*Δ cells, the nuclear Dcp2 localization was maintained even under stress conditions, while this effect was less noticeable in *edc3*Δ or *scd6*Δ cells. These data suggest that there might be a correlation between Dcp2 localization and the ability of the cell to form P-body granules.

Next, we asked whether the nuclear accumulation was specific for Dcp2 or whether other P-body components behaved in a similar manner in the absence of Edc3 and Scd6. Although Dcp1, which is part of the decapping complex, acted similarly to Dcp2, the exonuclease Xrn1 and the Lsm-associated protein Pat1 remained cytoplasmic (Fig. 1G–I). Of note, none of these proteins showed nuclear localization in the wild type (Fig. S1). Therefore, loss of Edc3 and Scd6 causes the selective nuclear accumulation of the decapping complex. Nevertheless, Pat1 had been shown previously to become localized to the nucleus in an *lsm1*Δ mutant (Teixeira and Parker, 2007). In addition, in mammalian cells, the interaction of Pat1 with both the splicing machinery in the cell nucleus and cytoplasmic P-bodies has been demonstrated (Vindry et al., 2017). However, Dcp2 was not enriched in the nucleus under the same conditions (Fig. 1I). Our data indicate that at least two independent pathways exist to control the cytoplasmic-nuclear distribution of a subset of P-body components.

Dcp2 uses two distinct NLSs and the karyopherin β Kap95 for nuclear localization

It is conceivable that Dcp2 depends on Dcp1 to be localized to the nucleus in *edc3*Δ *scd6*Δ cells. To test this possibility, we generated a triple deletion *edc3*Δ *scd6*Δ *dcp1*Δ. In this strain, Dcp2 still reached the nucleus (Fig. 2A), indicating that nuclear import does not depend on the assembled decapping complex and that Dcp2 itself must contain a nuclear import signal.

We analyzed the Dcp2 sequence with the NLStradamus model (Nguyen Ba et al., 2009) for NLS prediction and found three potential monopartite NLSs in the amino acid regions 450–467, 564–574 and 697–709 (Fig. S2A). The last region was also identified using cNLS Mapper, a web-based application for prediction of importin substrates (Kosugi et al., 2009), as a part of a moderately strong bipartite NLS spanning over amino acids 673–707 (Fig. S2B). In order to determine which of the NLSs was responsible for nuclear targeting, we introduced mutations that would abolish the function of the NLSs (Fig. 2B). While even the combination of mutations R565T, R566T, K569T, K571T and R573T (denoted S564T) and mutations K697T, K698T, K701T, K703T, K706T and R707T (denoted K697T) supported import of Dcp2 into the nucleus, Dcp2 with mutations K460T, K461T, K463T and K465T (denoted K450T) showed strongly reduced nuclear enrichment (Fig. 2C,D). Thus, Dcp2 contains at least one functional NLS that promotes nuclear import. However, some Dcp2-K450T still remained in the nucleus. We noticed that the RNA-binding site in Dcp2 also may contain an NLS (Fig. S2B). To test whether the RNA-binding site contained a cryptic NLS, we mutated three critical arginine residues in the R229 region, mutations R229T, R236T and R239T (denoted R229T). Indeed, this mutant reduced the nuclear accumulation of Dcp2 (Fig. 2C,D). Moreover, combining R229T with K460T resulted in an additive effect. The presence of the NLSs suggests the import might be mediated by the karyopherin α–karyopherin β (Kap60–Kap95) complex. Both *KAP60* and *KAP95* are essential for cell viability. Therefore, we tagged *KAP95* C-terminally with an auxin-inducible degron (AID) in *edc3*Δ *scd6*Δ cells to acutely deplete Kap95 upon addition of auxin. We observed, however, that import of Dcp2–GFP into the nucleus was already impaired in the absence of auxin, indicating that the addition of the degron resulted in a hypomorphic *kap95* allele (Fig. 2E,F). In fact, the addition of the AID to Kap95 results in lower Kap95 levels (Fig. S2C,D). This reduction in protein stability might be responsible for the reduced efficiency in nuclear import in general (Fig. S2E,F). Therefore, we conclude that Dcp2 contains two functional NLSs in which the function of one might be connected to the RNA-binding status of Dcp2. In addition, the nuclear localization of Dcp2 is dependent on karyopherin β.

The decapping complex is stored in the nucleus as a readily releasable pool

Next, we asked what could be the role of the decapping complex in the nucleus. Dcp1/2 could potentially decap mRNAs already in the nucleus and drive their decay there. Alternatively, the cytoplasmic concentration of active decapping complex might be tightly controlled and the nucleus would only serve as a storage space for any extra decapping complex. First, we explored a potential nuclear function of Dcp2. For this, we overexpressed GFP-tagged Dcp2 or a catalytically dead Dcp2 ($Dcp2^{CD}$) (Van Dijk et al., 2002) with or without the strong SV40 nuclear localization signal (NLS^{SV40}) (Fig. 3A; Fig. S3A,B). While high levels of $Dcp2^{CD}$ reduced cellular fitness over a range of temperatures, confining $Dcp2^{CD}$ to the nucleus, rescued this phenotype. Likewise, a high nuclear concentration of Dcp2 was not toxic (Fig. 3B). Our data suggest that Dcp2 has essential decapping functions in the cytoplasm but not in the nucleus. Moreover, high levels of nuclear Dcp2 are well tolerated, suggesting that Dcp2 may not be active in the nucleus.

Decapped RNA is unstable in the nucleus (Kufel et al., 2004). Our results above indicate that Dcp2 should not enhance RNA degradation in the nucleus. To this end, we detected polyA RNA in a *nup145*ΔC mutant, which is deficient for mRNA nuclear export at the restrictive temperature (Kufel et al., 2004). We did not detect any decrease in the polyA RNA signal by fluorescence *in situ* hybridization (FISH) under conditions when Dcp2 was sequestered in the nucleus either in the *edc3*Δ *scd6*Δ mutant or when we expressed

Journal of Cell Science (2021) 134, jcs259156. doi:10.1242/jcs.259156

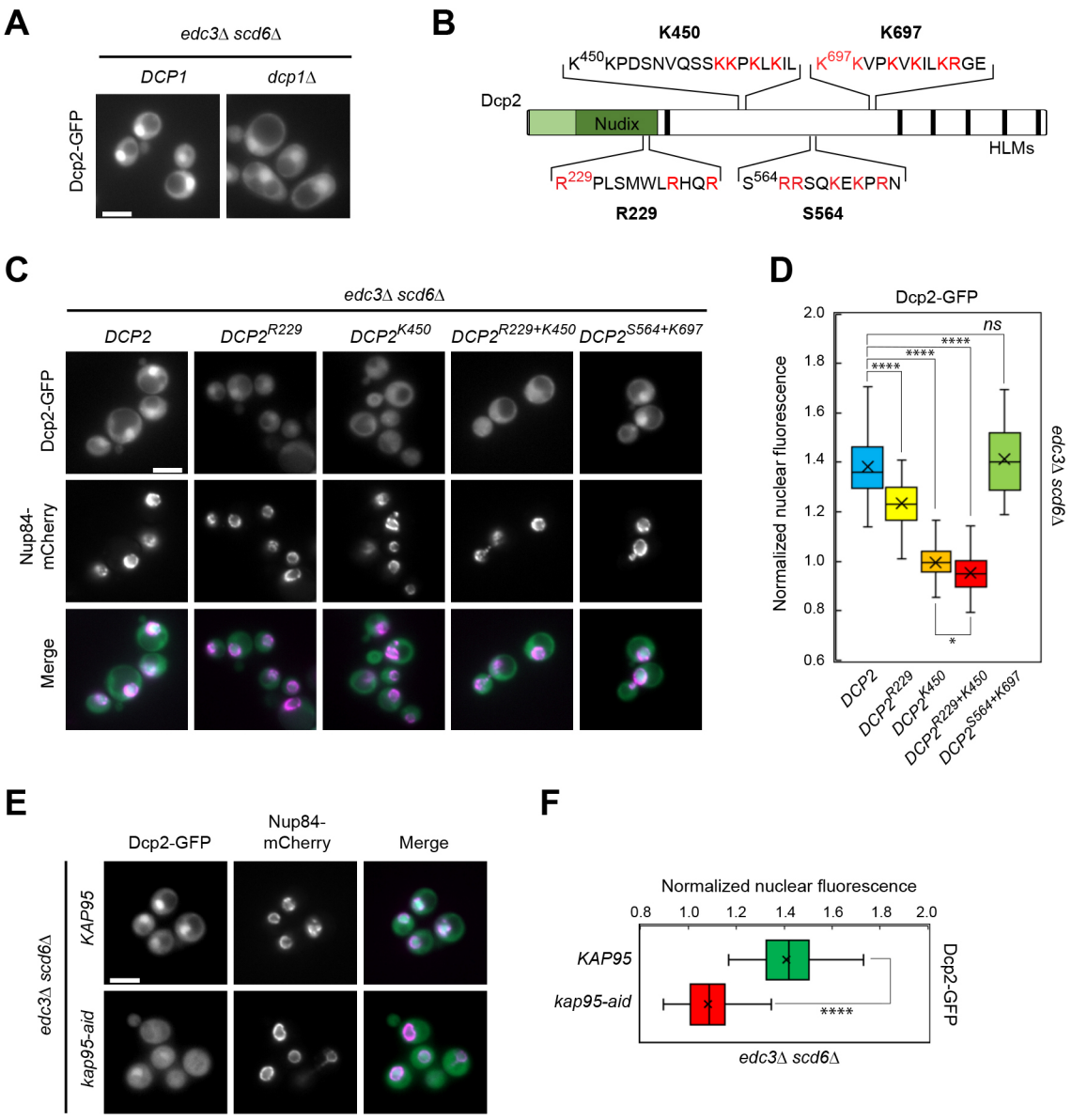

Fig. 2. Dcp2 uses two distinct NLSs and Kap95 for nuclear localization. (A) Dcp1 is not required for nuclear enrichment of Dcp2 in *edc3Δ scd6Δ*. Logarithmically growing cells expressing genomically tagged Dcp2-GFP were imaged without further treatment. Images representative of three experiments. Scale bar: 5 µm. (B) Four putative NLSs were identified in the *S. cerevisiae* Dcp2 protein sequence using NLStradamus and cNLS cutter web-based tools – three canonical (K450, S564 and K697) and one cryptic signal sequence (R229). The arginine or lysine residues indicated in red were mutated to threonine to test their involvement in the Dcp2 nuclear import. (C) The NLSs near K450 and R229 are responsible for the Dcp2 nuclear localization in *edc3Δ scd6Δ*. Cells with the genomically tagged nuclear marker Nup84–mCherry were transformed with low-copy plasmids bearing Dcp2–GFP with the indicated mutations. Logarithmically growing cultures were imaged without further treatment. Scale bar: 5 µm. (D) Quantification of the nuclear-cytoplasmic distribution of Dcp2-GFP from the data as shown in C. (E) Dcp2 nuclear import is dependent on Kap95. *KAP95* in *edc3Δ scd6Δ* cells expressing genomically tagged Dcp2–GFP and the nuclear marker Nup84–mCherry was C-terminally tagged with an auxin-inducible degron. Logarithmically growing cells from the starting strain and the *KAP95*-tagged variant were imaged without further treatment. Scale bar: 5 µm. (F) Quantification of the nuclear-cytoplasmic Dcp2-GFP distribution from the data as shown in E. Box plots in D and F are presented as described in the Materials and Methods. ****P<0.0001; n.s., not significant (P>0.05) (non-parametric test).

NLS^{SV40}-Dcp2–GFP, indicating that Dcp2 nuclear localization does not result in RNA instability (Fig. 3C–F). If at all, nuclear Dcp2 led to stabilization of polyA RNA. Moreover, an mRNA decay assay in which we assessed the decay of *MET3* mRNA also indicated that mRNA decay was not accelerated by nuclear Dcp2 (Fig. S3C–E). Therefore, we conclude that Dcp2 is not actively decapping nuclear mRNAs for decay under these conditions. Taken together, our data do not support a nuclear decay function for Dcp2 and are consistent with the notion that the nuclear Dcp2 pool may serve as a buffer to control cytoplasmic decapping activity.

If cytoplasmic Dcp2 levels are controlled and the nucleus acts as a buffer, we would expect to be able to send excess Dcp2 into the nucleus. In order to test this prediction, we first sequestered a pool of Dcp2 in the cytoplasm. Since P-bodies are associated with the endoplasmic reticulum (ER) (Kilchert et al., 2010; Weidner et al., 2014; Wang et al., 2018; Lee et al., 2020), we anchored Dcp2 to the ER by appending Dcp2–GFP to the ER protein Dpm1, denoted Dcp2–GFP^{ER} (Fig. S3F). In this strain, we also expressed Dcp2–2xmCherry which is soluble (Fig. 3G). In cells expressing Dcp2–GFP^{ER}, we observed Dcp2–2xmCherry in the nucleus, consistent with the notion

Journal of Cell Science (2021) 134, jcs259156. doi:10.1242/jcs.259156

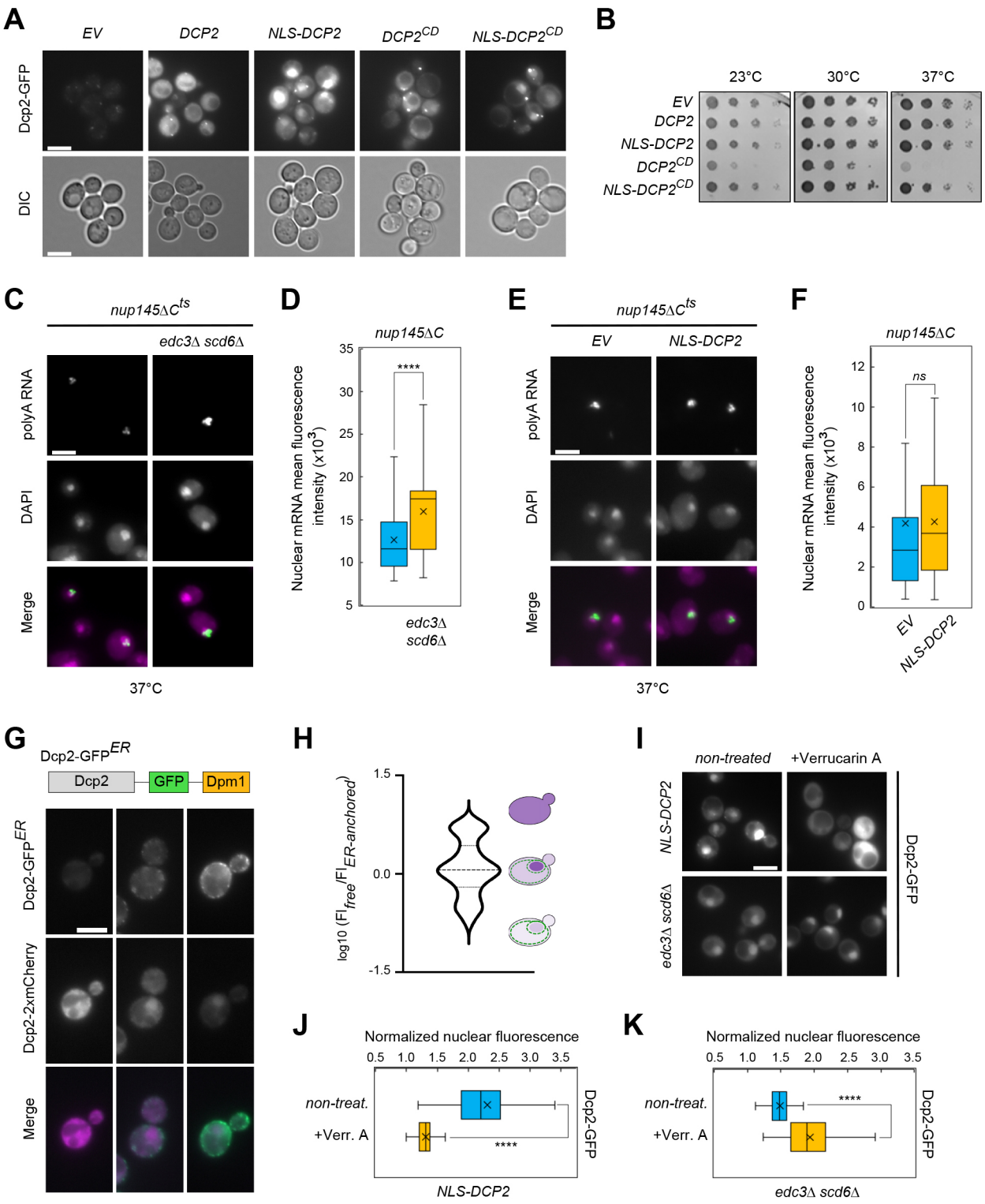

Fig. 3. See next page for legend.

that excess Dcp2 was sent to the nucleus. However, we also observed three distinct cell populations with different expression levels for both constructs. We observed either similar expression levels of Dcp2–GFP^{ER} and Dcp2–2xmCherry, or predominantly the expression of one of the constructs (Fig. 3H), indicating the presence of additional mechanisms contributing to the apparently tight control of the cytoplasmic Dcp2 protein levels.

If the nuclear Dcp2 were serving as a readily releasable pool, one would expect that we would observe a transition of Dcp2 from the nucleus into the cytoplasm under stress. To test this hypothesis, we expressed NLS^{SV40}-Dcp2–GFP, which localized Dcp2 efficiently to the nucleus (Fig. 3I,J). When we inhibited translation initiation with Verrucarin A (Fig. S3G), and hence provided an excess of 'free' mRNA in the cytoplasm, Dcp2–GFP was observed in the

Journal of Cell Science (2021) 134, jcs259156. doi:10.1242/jcs.259156

Fig. 3. The decapping complex is stored in the nucleus as a readily releasable pool. (A) Overexpression of NLS-appended and catalytically dead (CD) variants of Dcp2. Cells expressing Dcp2–GFP from a genomic locus were transformed with a low-copy plasmid expressing different versions of Dcp2–GFP from the strong *GPD* promoter. Cells from a logarithmically grown culture were imaged by fluorescence microscopy. *EV*, empty vector. Scale bars: 5 µm. (B) High levels of Dcp2 as well as Dcp2 sequestered in the cell nucleus do not affect cell fitness. Serial dilutions of the strains in A were spotted on YPD-agar, and incubated for 2 days at the indicated temperatures. Images in A and B are representative of three experiments. (C–F) Increased levels of nuclear Dcp2 do not enhance nuclear mRNA degradation. The *nup145*ΔC strain background was either deleted for *EDC3* and *SCD6*, or transformed with low-copy plasmid expressing the NLS–Dcp2. Logarithmically growing cultures were shifted to 37°C to inhibit mRNA nuclear export, fixed and the amount of nuclear polyA mRNA was assessed by *in situ* hybridization with a Cy3-oligo(dT) probe. The cell nucleus was stained with DAPI. Scale bars: 5 µm. (D,F) Quantification of the mean fluorescence of the nuclear polyA mRNA. (G) Cytoplasmic Dcp2 levels are tightly regulated through targeting to the cell nucleus and/or degradation. Cells with genomically tagged Dcp2–2xmCherry were transformed with a low-copy plasmid expressing Dcp2–GFP–Dpm1 for anchoring at the cytosolic face of the ER from the DCP2 promoter. Logarithmically growing cultures were imaged without treatment. Scale bar: 5 µm. (H) Quantification of the total mCherry and GFP fluorescence of the cells as shown in G; 92 cells from three biological replicates were quantified. Results are presented as a violin plot with median and interquartile range indicated. (I–K) Dcp2 can be released from its nuclear pool upon increased demand in the cytoplasm only in the presence of Edc3 and Scd6. Wild-type cells expressing NLS–Dcp2–GFP from a strong promoter or *edc3*Δ *scd6*Δ cells expressing genomically tagged Dcp2–GFP were imaged upon treatment with 25 µg/ml verrucarin A in a rich medium for 1 h at 30°C. Scale: bar 5 µm. Box plots in D, F, J and K are presented as described in the Materials and Methods. ****P<0.0001; n.s., not significant (P>0.05) (non-parametric test).

cytoplasm, indicating that even the strong SV40 NLS was overridden (Fig. 3I,J). As a control for these experiments, we depleted Dcp2 by means of an auxin-inducible degron (Fig. 4F). To our surprise, we observed a decrease in translation under these conditions (Fig. S3I). This phenotype was not observed when we expressed NLS^{SV40}-Dcp2–GFP in the same strain background (Fig. S3J). Both sets of experiments are consistent with the notion that nuclear Dcp2 could serve as readily releasable pool.

On the other hand, this meant at least one factor must sequester Dcp2 in the cytoplasm to avoid reimport into the nucleus. This cytoplasmic sequestering function is provided by Edc3 and Scd6 because in an *edc3*Δ *scd6*Δ strain, NLS^{SV40}-Dcp2–GFP remained nuclear when translation was attenuated; even more Dcp2 accumulated in the nucleus (Fig. 3I,K; Fig. S3H).

Dcp1/2 performs essential functions on the cytoplasmic face of the ER

Another prediction from our model that nuclear Dcp2 serves as a readily releasable pool is that the essential function of Dcp2 should be in the cytoplasm, in particular under stress conditions, when P-bodies are formed. We have previously shown that *BSC1* mRNA and *ILM1* mRNA both localize to P-bodies, and although *BSC1* mRNA was degraded under glucose starvation, *ILM1* mRNA was stabilized (Wang et al., 2018). When we depleted Dcp2 using an AID, *BSC1* mRNA was stabilized and even increased during the time course of the experiment (Fig. 4A). This stabilization was reversed when we expressed NLS^{SV40}-Dcp2–GFP, indicating that nuclear localized Dcp2 could exit the nucleus to become integrated into P-bodies and decap *BSC1* mRNA. As expected, *ILM1* mRNA was unaffected by changes in Dcp2 levels under the same conditions. This Dcp2 integration into P-bodies may depend on Edc3 and Scd6. Indeed, an *edc3*Δ *scd6*Δ mutant, in which Dcp2 becomes sequestered in the nucleus, showed impaired growth under stress (Fig. 4B). If this growth impairment was solely due to the Dcp2 localization, then Dcp2 overexpression (Fig. 4C,D) should rescue the growth defect. Overexpression of Dcp2 alleviated the growth phenotype of the *edc3*Δ *scd6*Δ mutant strain (Fig. 4E). These data indicate that Edc3 and Scd6 collaborate to regulate cytoplasmic Dcp2 levels, and that excess Dcp2 can be stored in the nucleus until needed.

The simple overexpression method, however, has two drawbacks. First, it increases the entire cytoplasmic pool of Dcp2 without providing spatial information and, second, the overexpressed protein can still be imported and trapped in the cell nucleus. To circumvent these potential pitfalls, we locked Dcp2 in the cytosol. To this end, we anchored Dcp2–GFP on the cytosolic face of the ER and of mitochondria (MITO) by linking Dcp2–GFP to Dpm1 ($Dcp2^{ER}$) or Fis1 ($Dcp2^{MITO}$) (Figs S3F and S4A,B). The mitochondrial targeting was chosen as a control as we predicted, based on our previously published results, that mitochondrial Dcp2 would not be functional (Kilchert et al., 2010; Weidner et al., 2014; Wang et al., 2018). Dcp2 appended with Fis1 localized efficiently to mitochondria. The two constructs, $Dcp2^{ER}$ and $Dcp2^{MITO}$ were expressed at similar levels (Fig. S4C,D). To ensure that the endogenous Dcp2 would not interfere with our assay, we acutely depleted endogenous Dcp2 using an AID. This depletion worked efficiently, as even under normal growth conditions Dcp2-depleted *edc3*Δ *scd6*Δ cells were unable to grow (Fig. 4F). Under these conditions, however, both mitochondrial and ER-localized Dcp2 rescued the growth phenotype. Under stress conditions, the ER-sequestered Dcp2 allowed much better survival when compared to Dcp2 on mitochondria (Fig. 4F). This was also observed when $Dcp2^{ER}$ and $Dcp2^{MITO}$ were expressed from a high copy vector (Fig. S4E). Therefore, the ER-localized Dcp2 pool is chiefly responsible for the response to stress. These findings also suggest that functional P-body formation does not occur randomly in the cytoplasm, but is rather restricted to specific sites at ER membranes.

Nevertheless, we observed also some rescue mediated by the mitochondria-localized Dcp2. To understand these results better, we first tested whether P-bodies could be formed on mitochondria under stress conditions. Indeed, $Dcp2^{MITO}$ formed foci resembling P-bodies under glucose starvation (Fig. 4G). These foci were also positive for two other bona fide P-body components, Dhh1 and Pat1 (Fig. S4F,G), indicating that P-bodies can also form on mitochondria. Moreover, our data suggest that Dcp2 alone is sufficient to determine the location of P-body formation.

The ER and mitochondria are connected via contact sites to allow the exchange of lipids and ions (Elbaz and Schuldiner, 2011; Prinz, 2014). In yeast, the tethering complex ERMES stabilizes these contacts (Kornmann et al., 2009). We wondered whether the P-bodies formed containing $Dcp2^{MITO}$ would be localized close to ER–mitochondria contact sites. Indeed, P-bodies were detected next to or at the same site as the ERMES component Mdm34 (Fig. 4H,I). This presence at ER–mitochondria contact sites was essential for the ability of $Dcp2^{MITO}$ to mount an appropriate stress response because destruction of the contacts by deleting the ERMES component Mmm1 abolished growth of $Dcp2^{MITO}$-expressing cells under stress (Fig. 4J) without changing the $Dcp2^{MITO}$ levels (Fig. S4H,I). Taken together, our data are consistent with the notion that functional P-body formation under stress takes place at the ER and not randomly in the cytoplasm. Moreover, our data provide evidence that Dcp2 and P-bodies can also act in trans to cope with stress at ER–mitochondrial contact sites, albeit somewhat less efficiently.

Journal of Cell Science (2021) 134, jcs259156. doi:10.1242/jcs.259156

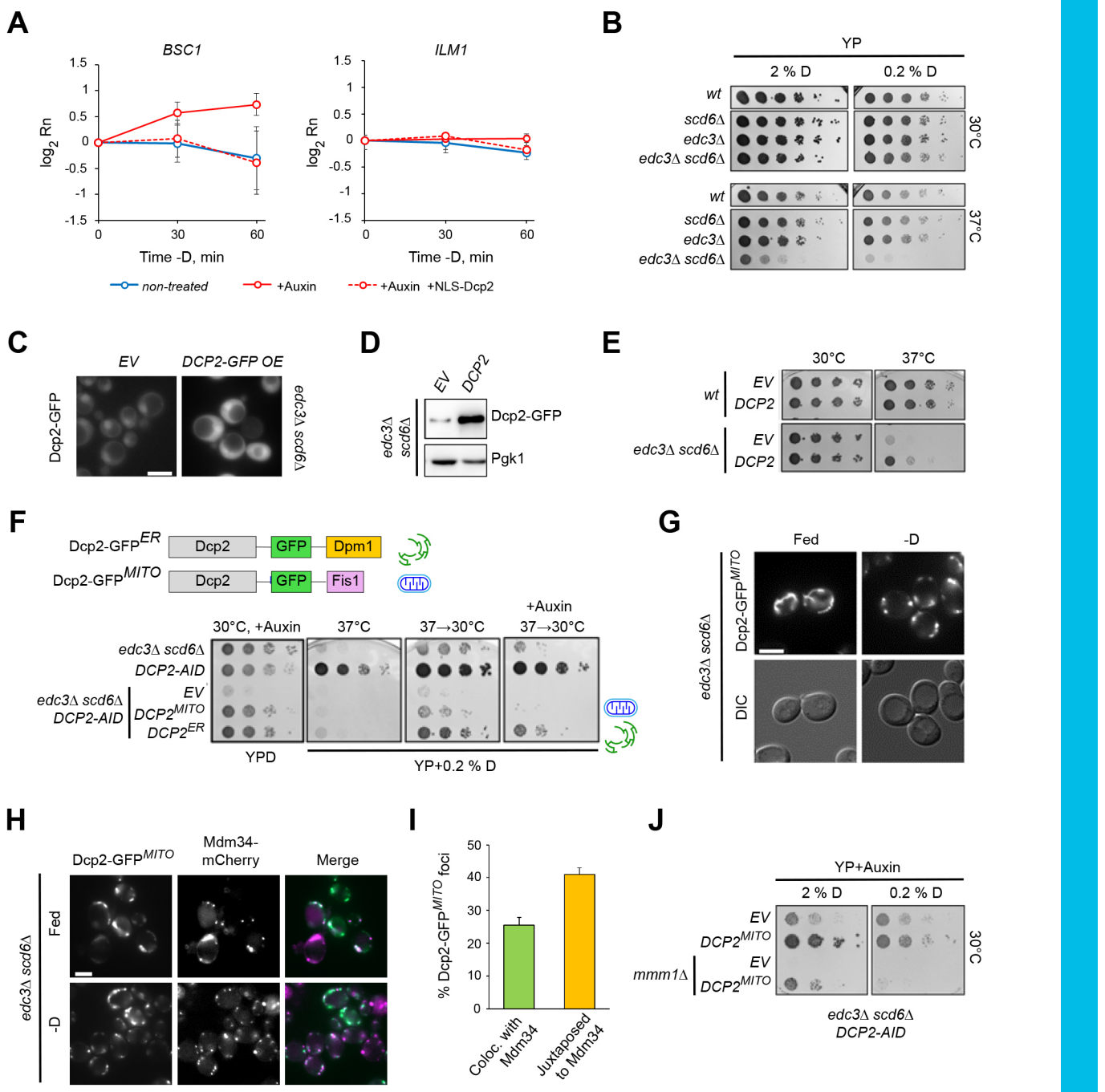

Fig. 4. See next page for legend.

Scd6 and Edc3 bridge the interaction of Dcp2 with Dhh1 during P-body assembly

Our data above suggest that Dcp2 localization determines where P-bodies assemble. Dcp2 can interact with both Scd6 and Edc3 (Fig. 5A), which in turn also interact with Dhh1, although their binding to Dhh1 was reported to be mutually exclusive (Fromm et al., 2012). Importantly, Dhh1 has been shown to drive phase separation, which is essential during P-body formation (Mugler et al., 2016; Hondele et al., 2019). First, we wanted to determine which domains of Scd6 and Edc3 are required to keep Dcp2 in the cytoplasm and to promote functional stress response. To this end, we carried out a domain analysis of Scd6 and Edc3 by overexpressing their individual domains alone or in combination in the *edc3*Δ *scd6*Δ background and determined the nuclear-cytoplasmic distribution of Dcp2 and fitness at 37°C (Fig. 5B–E; Fig. S5A,B). As reported previously, overexpressing full-length Scd6 impaired growth due to constitutive P-body formation, even without stress (Nissan et al., 2010). Removal of the C-terminal region of Scd6 or Edc3 not only alleviated these growth defects, but restored growth to wild-type levels and reversed the P-body phenotype. Scd6 or Edc3 constructs lacking either the Dhh1 or the Dcp2 interaction site failed to restore growth, and Dcp2 became enriched in the nucleus. On the other hand, the LSm domain of either Edc3 or Scd6, which interacts with Dcp2 was sufficient to

Journal of Cell Science (2021) 134, jcs259156. doi:10.1242/jcs.259156

Fig. 4. Dcp1/2 performs essential functions on the cytoplasmic face of the ER. (A) NLS-Dcp2 is released into the cytoplasm under stress to destabilize specific mRNAs targeted to P-bodies. NLS–Dcp2 was expressed in a strain with *DCP2* tagged genomically with an auxin-inducible degron. Upon metabolic labelling of RNA with 4-thiouracil (4TU) and depletion of Dcp2-AID with auxin the cultures were starved for glucose (-D) and chased with excess uracil. 4TU-labelled RNA was biotinylated and purified, and the levels of the *BSC1* and *ILM1* labelled transcripts were determined by qRT-PCR using *ACT1* as a reference. Results are mean±s.d. for four experiments. (B) *edc3*Δ *scd6*Δ displays impaired growth under stress. Serial dilutions of the indicated strains were spotted on YP-agar containing 2 or 0.2% glucose (marked as D), and incubated at 30°C or 37°C for 2 days. *wt*, wild type. (C,D) Dcp2 overexpression in *edc3*Δ *scd6*Δ. Dcp2–GFP was expressed on a *GPD* promoter from a low-copy plasmid on top of genomically tagged Dcp2-GFP in *edc3*Δ *scd6*Δ. Logarithmically growing cells were either imaged directly (C) or GFP expression was analyzed by western blotting (D). Scale bar: 5 µm. (E) Overexpression of Dcp2 partially rescues growth of *edc3*Δ *scd6*Δ under stress. Wild-type and *edc3*Δ *scd6*Δ strains expressing Dcp2–GFP on a *GPD* promoter from a low-copy plasmid were serially diluted and spotted on YPD-agar, and incubated at the indicated temperatures for 2 days. (F) Dcp2 at the ER is required for growth under stress. *edc3*Δ *scd6*Δ with *DCP2* tagged genomically with an auxin-inducible degron were transformed with low-copy plasmids expressing the indicated Dcp2-constructs from the endogenous *DCP2* promoter. Serial dilutions of the respective logarithmically growing cultures were spotted on YP-agar with 2 or 0.2% glucose, and supplemented with 0.2 M auxin as indicated. Agar plates were incubated either for 2 days at 30°C or first for 2 days at 37°C, and then for 3 days at 30°C. (G) $Dcp2^{MITO}$ forms foci upon glucose starvation. *edc3*Δ *scd6*Δ strain with the endogenous *DCP2* tagged with an auxin-inducible degron was transformed with a low-copy plasmid expressing the $Dcp2^{MITO}$ construct from a *DCP2* promoter. Logarithmically growing cultures were treated with 2 mM auxin for 2 h, and either imaged directly or upon 30 min glucose deprivation. Scale bar: 5 µm. Images in B–G are representative of three experiments. (H) $Dcp2^{MITO}$ foci localize in close vicinity of ER-mitochondria contact sites. *edc3*Δ *scd6*Δ strain with genomically tagged Mdm34–mCherry and Dcp2-AID was transformed with a low-copy Dcp2–GFP^{MITO} construct. Logarithmically growing cells were treated as for panel 3F. Scale bar: 5 µm. (I) Quantification of the number of GFP foci in panel 3H colocalizing or juxtaposed to Mdm34 upon 30 min of glucose starvation. Results are mean±s.d. for three experiments. (J) ER–mitochondria contact sites are essential for the functioning of $Dcp2^{MITO}$ under stress. *edc3*Δ *scd6*Δ with the endogenous *DCP2* tagged with an auxin-inducible degron was deleted for *MMM1* and transformed with a low-copy plasmid expressing $Dcp2^{MITO}$ from a *DCP2* promoter. Logarithmically growing cultures of the indicated strains were serially diluted and spotted on YP-agar with 2% or 0.2% glucose, supplemented with 0.2 M auxin, and incubated at 30°C for 3 days. Images representative of three experiments.

induce P-body formation when anchored at the ER (Fig. S5C,D). Our data demonstrate that both Scd6 and Edc3 can bridge the interaction between Dcp2 and Dhh1, and that this connection is needed to keep Dcp2 from being transferred into the nucleus.

Linking Dcp2 and Dhh1 drives P-body formation and a functional stress response

So far, our data suggest that Dcp2 and Dhh1 must come together to drive P-body formation under stress and that this process is mediated through interaction with either Scd6 or Edc3. To further corroborate our findings, we fused the N-terminal Dcp2 binding domain of Edc3 ($Edc3^{1\text{-}86}$) to Dhh1 and expressed the construct in the *edc3*Δ *scd6*Δ Dcp2–GFP strain (Fig. 6A; Fig. S6A). Consistent with the data described above, Dcp2 was mostly nuclear in *edc3*Δ *scd6*Δ cells (Fig. 6B,C). This localization did not change when Dhh1 was expressed separately. Consistent with the data above (Fig. 5B,C), the expression of the $Edc3^{1\text{-}86}$ domain alone led only to partial rescue of Dcp2 cytoplasmic localization. However, the expression of the $Edc3^{1\text{-}86}$–Dhh1 fusion protein sequestered Dcp2 in the cytoplasm, and Dcp2 co-precipitated with $Edc3^{1\text{-}86}$–Dhh1, but not with Dhh1 (Fig. 6B; Fig. S6B). More importantly, when we assessed Dcp2 localization under glucose starvation, expression of only $Edc3^{1\text{-}86}$–Dhh1 was sufficient to induce P-body formation (Fig. 6D,E). These P-bodies appear to be functional as they completely rescued the growth phenotype of *edc3*Δ *scd6*Δ (Fig. 6F).

Dcp2 is required for functional P-body assembly

Our above data suggest that Dcp2 promotes P-body formation. However, it is assumed that P-body assembly is redundant and no single component is essential (Teixeira and Parker, 2007). Therefore, we decided to revisit the issue and determined P-body formation in our Dcp2-AID degron strain. Similar to what had been described previously (Teixeira and Parker, 2007), upon Dcp2 depletion, P-body formation was strongly impaired (Fig. 7A,B). Instead of 1–3 bright foci/cell, either only diffuse signal or multiple weak foci were observed, which were most conspicuous in the case of Edc3. To test whether these smaller foci might present smaller functional P-body units, we performed colocalization analyses. While Edc3 colocalized with Xrn1 and Pat1 very well in the presence of Dcp2, this level of colocalization dropped drastically in the absence of Dcp2 (Fig. 7C–E). Therefore, we conclude that, even though smaller speckles can be formed in the absence of Dcp2, they do not represent functional P-bodies, indicating that Dcp2 is essential for functional P-body formation. Moreover, our data are in accordance with previous data (Weidner et al., 2014) showing that granule formation and phase separation do not necessarily correlate with P-body functionality.

DISCUSSION

Even though P-bodies are an essential part of the cellular stress response, their assembly and cellular location are still debated and not fully understood. Recent studies have highlighted the dynamics of individual P-body components during and the removal after stress (Xing et al., 2020; Lee et al., 2020). The mechanism of their formation, however, is still not entirely clear. Edc3 and Lsm4 have been shown to function in P-body assembly (Decker et al., 2007). In a more recent study, it was shown that the phase separation capability of the helicase Dhh1 contributed to P-body formation (Hondele et al., 2019). Yet, the dogma in the field is that no individual P-body component is essential for P-body formation. This reasoning is largely based on a study in which all major P-body components were individually deleted and the formation of foci with individual P-body members was analyzed (Teixeira and Parker, 2007) with a recent follow up from the same group (Rao and Parker, 2017). The initial systematic study showed that none of the deletions completely suppressed foci formation. Here, we show that even though some P-body components form speckles in the absence of Dcp2, these appear not to be functional P-bodies as they lack other P-body components. Moreover, our data provide strong evidence that functional P-bodies are formed at the ER under stress, and not at some random place in the cytoplasm. We envisage an assembly pathway in which Dcp2 is associated with the ER through polysomes and/or other means. We have shown previously that a phosphorylated form of Dcp2 is enriched on ER-associated polysomes under normal growth conditions (Weidner et al., 2014). Moreover, immunoelectron microscopy has shown P-bodies localizing in close proximity to the ER under stress (Kilchert et al., 2010; Weidner et al., 2014), confirmed by a recent live-cell imaging approach in mammalian cells (Lee et al., 2020). Another P-body component, Scd6 is associated with polysomes in the cytoplasm and on ER membranes (Weidner et al., 2014), consistent with its role as a translational repressor. Upon stress, Scd6 would inhibit translation

Journal of Cell Science (2021) 134, jcs259156. doi:10.1242/jcs.259156

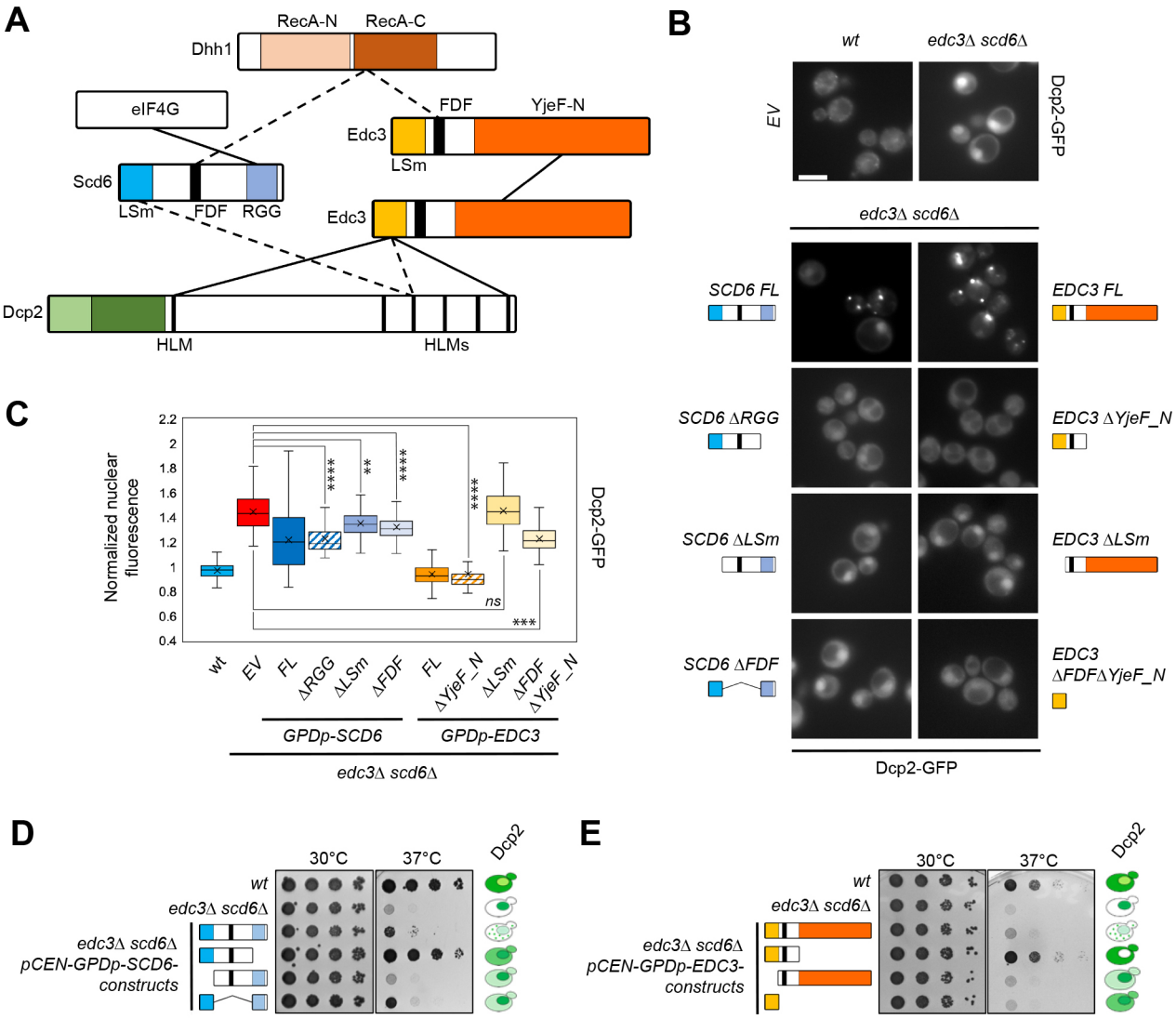

Fig. 5. Scd6 and Edc3 bridge the interaction of Dcp2 with Dhh1 during P-body assembly. (A) Schematic representation of the domain structure and interactions of Scd6, Edc3, Dcp2 and Dhh1. Dashed lines represent mutually exclusive interactions. (B) Bridging Dcp2 to Dhh1 is required to keep Dcp2 in the cytoplasm. Wild-type (*wt*) or *edc3Δ scd6Δ* cells with genomically tagged Dcp2–GFP were transformed with low-copy plasmids expressing the indicated *SCD6* or *EDC3* constructs from the strong *GPD* promoter. Logarithmically growing cells were imaged without further treatment. *EV*, empty vector. Scale bar: 5 µm. (C) Quantification of the nuclear-cytoplasmic GFP distribution in the cells as shown in B. Box plots are presented as described in the Materials and Methods. ***P*<0.01; ****P*<0.001; *****P*<0.0001; n.s., not significant (*P*>0.05) (non-parametric test). (D,E) Scd6 and Edc3 bridge Dcp2 to Dhh1 to cope with stress. Logarithmically growing cultures from the strains as shown in B were serially diluted and spotted on HC-agar lacking leucine, and incubated at 30 or 37°C for 2 days. The cartoon shows the Dcp2-GFP nuclear-cytoplasmic distribution. Images representative of three experiments.

either through its direct interaction with eIF4G, or with the help of Dhh1, which likewise has translational suppressor activity (Coller and Parker, 2005; Zeidan et al., 2018). However, in order to form a P-body, the local concentration of Scd6–Dhh1–mRNA complexes must be increased. This is achieved through binding to Dcp2 on the ER membrane (Fig. 8). We surmise that, on the membrane, which reduces the diffusibility of the Dcp2–Scd6–Dhh1–mRNA complexes, it is much easier to gain a critical concentration to initiate Dhh1-driven phase separation. In a next step, Edc3, which, like Scd6, can bind both Dcp2 and Dhh1 is recruited. Because Edc3 is a dimer, it can act as a scaffold to further enhance recruitment of Dhh1 and P-body formation. In our model, the local concentration of Dcp2 on ER polysomes would be key to driving P-body formation through this pathway. In support of our model, we find that first $Dcp2^{ER}$ can rescue a *scd6Δ edc3Δ* mutant, while $Dcp2^{MITO}$ cannot, unless concentrated at ER–mitochondrial contact sites. Second, directly linking Dcp2 to Dhh1 through the N-terminus of Edc3 ($Edc3^{1\text{-}82}$–Dhh1) is sufficient for cells to cope with stress. Moreover, an mRNA coupled to Scd6 is on the one hand translationally repressed in a Dhh1-dependent manner and on the other hand destabilized by Dcp2 (Zeidan et al., 2018), supporting the idea that there is a temporal control in P-body assembly. In agreement with this notion, Scd6 and Edc3 interact with Dcp2 and Dhh1 in a mutually exclusive manner (Decker et al., 2007; Harigaya et al., 2010; Nissan et al., 2010; Fromm et al., 2012; Sharif et al., 2013). Finally, a recent finding did not even consider Scd6 an abundant P-body component after prolonged stress (Xing et al., 2020), again supporting the idea that Scd6 plays an important role early in P-body assembly and may then be displaced by Edc3 over time. Yet, Scd6 is a bona fide P-body component because tagged Dcp2 and Scd6 are about equally efficient in purifying P-bodies and in determining the RNA content upon acute stress conditions (Weidner et al., 2014; Wang et al., 2018).

Journal of Cell Science (2021) 134, jcs259156. doi:10.1242/jcs.259156

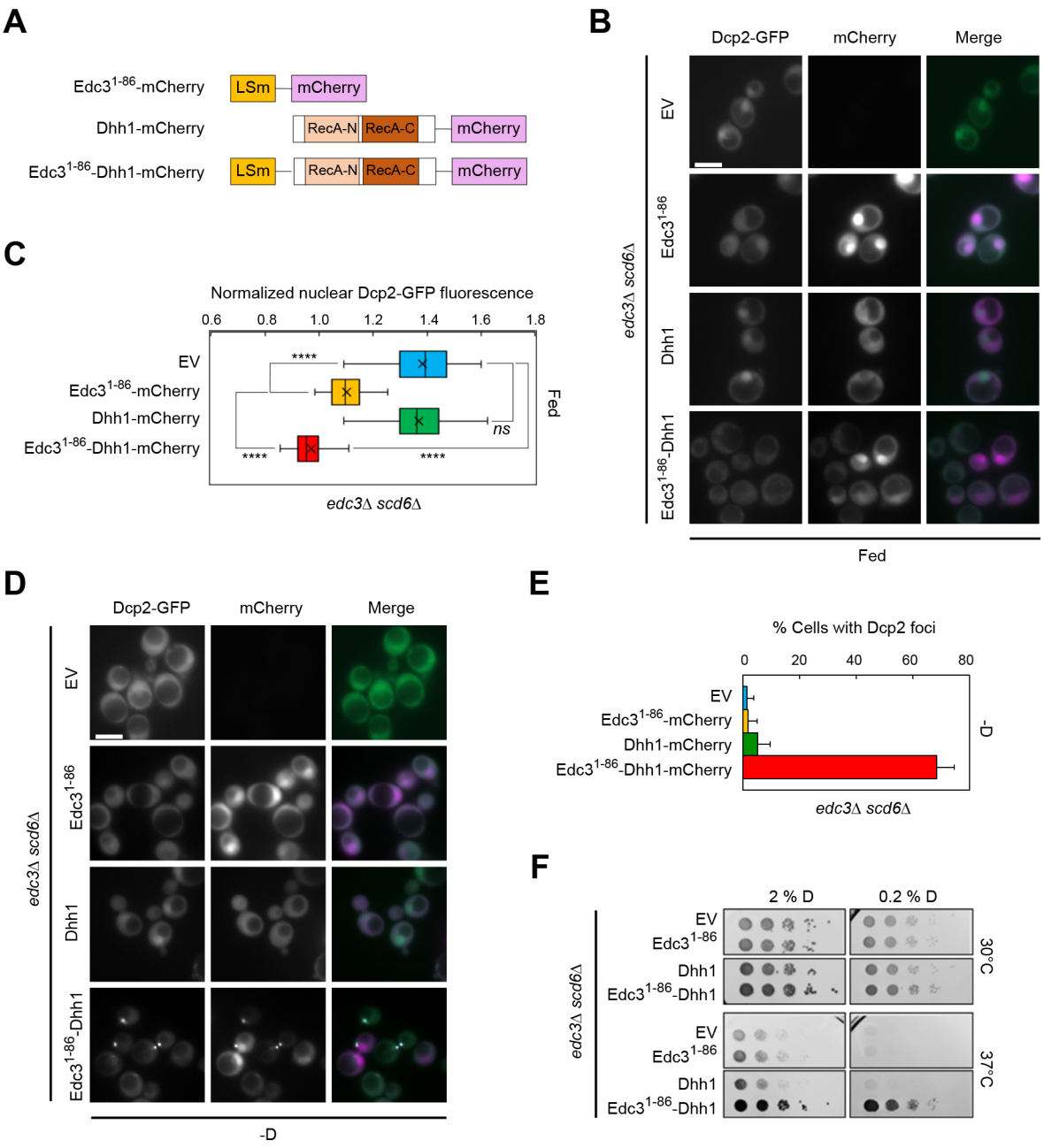

Fig. 6. Linking Dcp2 and Dhh1 drives P-body formation and the functional stress response. (A) Structure of the Edc3$^{1-86}$–Dhh1–mCherry fusion and the control Edc3$^{1-86}$–mCherry and Dhh1–mCherry constructs. All constructs were expressed from a low-copy plasmid on the endogenous *DHH1* promoter. (B–E) Linking Dhh1 to Dcp2 rescues the cytoplasmic localization of Dcp2 and P-body formation in *edc3*Δ *scd6*Δ cells. *edc3*Δ *scd6*Δ cells with genomically tagged Dcp2–GFP were transformed with the constructs from A. *EV*, empty vector. Logarithmically growing cells were imaged either directly (B) or after 30 min of glucose deprivation, denoted -D (D). Scale bars: 5 µm. (C) Quantification of the nuclear-cytoplasmic Dcp2–GFP distribution for cells as shown in B. Box plot is presented as described in the Materials and Methods. ****P<0.0001; n.s., not significant (P>0.05) (non-parametric test). (E) Quantification of the number of cells forming GFP foci upon 30 min of glucose deprivation (-D). (F) The Dcp2–Dhh1 interaction insures cell fitness under increased stress. Serial dilutions of the strains from panel B and C were spotted on YP-agar with 2 or 0.2% glucose, and incubated at the indicated temperatures for 2 days. Images representative of three experiments.

How does our model explain why deletions of, for example, *PAT1* and *LSM1* also affect P-body assembly? We propose that there is an initiation phase, and this is largely the process described above in which translational repression is intimately coupled to the initiation of P-body formation. In the next step, these molecular assemblies need to grow and to be stabilized, during which those P-body components associated with the 3′ of the client mRNA are needed. In our view, in *pat1*Δ and *lsm1*Δ cells, the initial assembly of the 5′ P-body members with the RNA at the ER is not defective, but rather stabilization of the assembly and its growth is disrupted. In this phase of P-body stabilization, the numerous partially redundant interactions among different P-body members are important, as previously described (Rao and Parker, 2017). Within 5 min of stress, such as glucose deprivation, P-bodies are formed. In particular under glucose starvation, multiple P-bodies initially become visible that apparently coalesce over 30 min. Thus,

Journal of Cell Science (2021) 134, jcs259156. doi:10.1242/jcs.259156

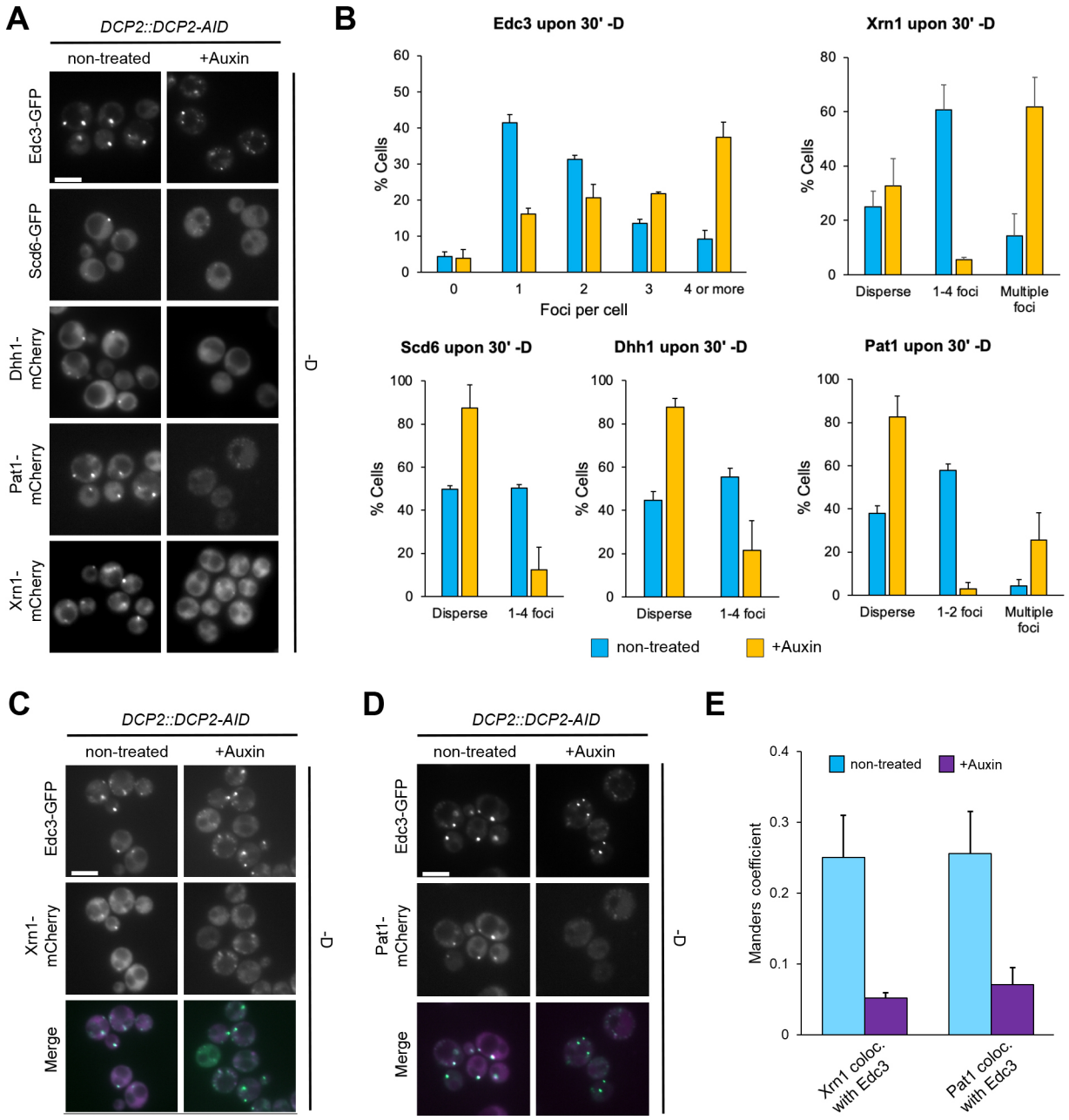

Fig. 7. Dcp2 is essential for P-body assembly. (A,B). Depletion of Dcp2 impairs P-body formation. All strains were constructed from an isogenic background with *DCP2* genomically tagged with an auxin-inducible degron. The respective genes were either genomically appended with GFP or mCherry at the C-terminus (*EDC3*, *SCD6* and *XRN1*), or the respective mCherry-tagged protein was expressed from a low-copy plasmid on its endogenous promoter (Dhh1 and Pat1). Logarithmically growing cells were treated with 2 mM auxin for 2 h, then deprived from glucose for 30 min (30′ -D) and imaged (A), and the number of mCherry foci was quantified (B). Scale bar: 5 µm. (C–E) Dcp2 coordinates the recruitment of Xrn1 and Pat1 to Edc3 during P-body formation. The strains expressing Edc3–GFP as in A were genomically tagged with mCherry at the *XRN1* locus (C) or transformed with a low-copy plasmid expressing Pat1–mCherry from its endogenous promoter (D). Logarithmically growing cells were treated as in A. Scale bars: 5 µm. (E) Manders coefficients for the fraction Xrn1–mCherry or Pat1–mCherry colocalizing to Edc3–GFP upon 30 min of glucose deprivation (-D). Results in B and E are mean±s.d. for three experiments.

P-bodies seem to mature over time, perhaps also becoming more stable entities under non-adaptable stress conditions, such as glucose starvation. In contrast, under adaptable stresses, this maturation process might be less critical, in particular if cells can reach a new equilibrium state within 30–45 min and start to dissociate P-bodies, as under hyperosmotic stress conditions (Kilchert et al., 2010).

If Dcp2 localization, and presumably activity, are critical for P-body formation, they should be strongly controlled. We know that the activity of Dcp2 can be regulated by phosphorylation and Edc3 (EDC4 in mammals) binding (Harigaya et al., 2010; Yoon et al., 2010; Chang et al., 2014; Paquette et al., 2018). Besides these on-and-off switches of activity, the cell might still want to control the protein localization as a second line to control activity. Upon stress, more Dcp2 would be needed immediately to cope with the remodeling of the proteome. Acute stress demands an acute response in which a reserve or buffering pool would be advantageous. This pool may be sequestered away from the cytoplasm in order to prevent

Journal of Cell Science (2021) 134, jcs259156. doi:10.1242/jcs.259156

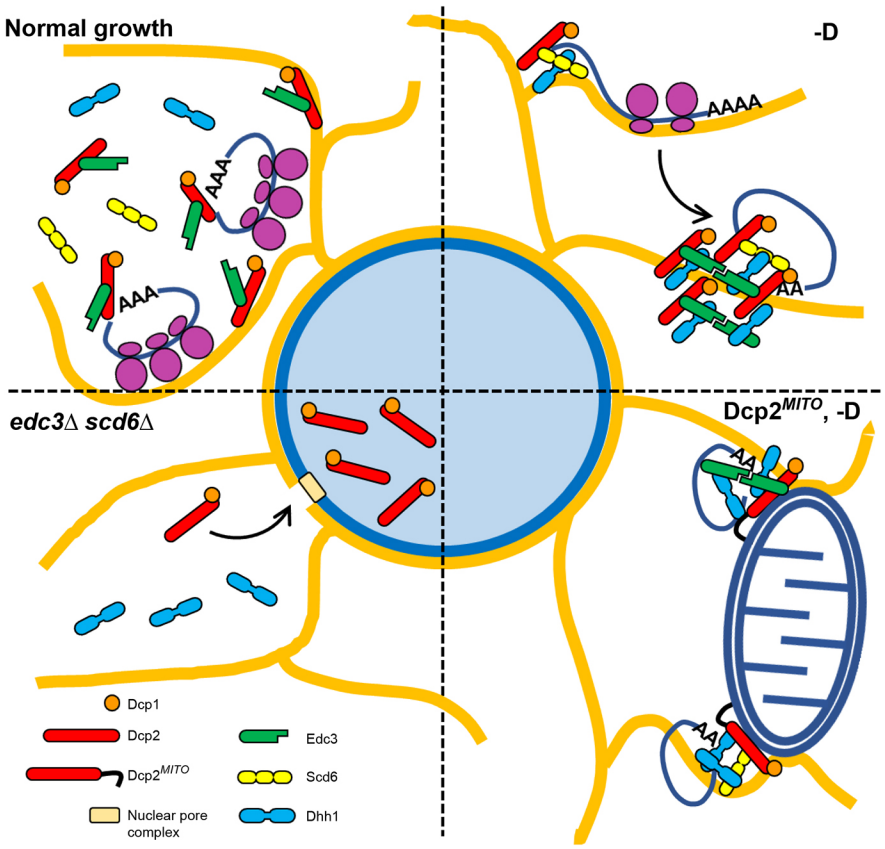

Fig. 8. Schematic representation of our findings. Under normal growth conditions, mRNA translation on ribosomes (purple) occurs in the cytoplasm or on the ER (orange). Under starvation, translation is attenuated and P-bodies form at the ER. Anchoring the decapping complex on mitochondria, P-body formation occurs at ER-mitochondria contacts. In the absence of the P-body components Scd6 and Edc3, the decapping complex relocates into the nucleus (blue sphere). For detailed information, see the main text.

premature activation and to provide a more tuned response. Excess cytoplasmic Dcp2 might be recognized, on one hand, by the free RNA-binding site, which in turn could act as an NLS and contribute to Dcp2 nuclear localization through Kap95-dependent import. On the other hand, nuclear-cytoplasmic localization is also determined by the presence of Scd6 and Edc3, binding of which might likewise mask the other NLS. Thus, the nuclear-cytoplasmic distribution of the decapping complex is primarily regulated by two different NLSs, providing two independent readouts – RNA client availability and ability to bind to Edc3 and Scd6.

Nuclear Dcp2 does not appear to be engaged in nuclear mRNA decay. However, it has been previously reported that nuclear Dcp2 can act as a transcriptional activator (Haimovich et al., 2013). Nevertheless, the essential function of Dcp2 appears to be in the cytoplasm as overexpression of catalytically dead Dcp2 was detrimental but it had no effect when locked in the nucleus. Dcp2 is not the only P-body component that can be localized to the nucleus. The other, perhaps best documented, component is Pat1 (Teixeira and Parker, 2007). Intriguingly, overexpression of Pat1 drives nuclear localization of Dhh1 (Sachdev et al., 2019). It appears as if the nuclear-cytoplasmic distribution of key P-body components contributes to a built-in robustness to control cytoplasmic mRNA decay.

We propose that the arrangement of the mRNA decaying factors is orchestrated around Dcp2. Dcp2 may serve as a platform for organizing the different elements of the mRNA machinery on a modular principle. It associates with Scd6 and Edc3, which contact the major regulator Dhh1 responsible for liquid–liquid phase separation. An ensemble of activators (Dcp1, Edc1, Edc2, Edc3, Pat1 and Lsm1-7) acts concertedly to stimulate decapping. The downstream exonuclease Xrn1 recruited to the complex by Pat1 ensures the final processing of the transcript. Liquid–liquid phase separation and condensate formation can also take place in the absence of Dcp2. The lack of the decapping platform, however, leads to loss of spatial and temporal coordination of the mRNA decay factors and failure to properly organize in P-bodies under stress. This process is likely to be conserved in mammalian cells, because the Dhh1 homolog DDX6 promotes also phase separation (Hondele et al., 2019) and the cryptic NLS in the Dcp2 RNA-binding site also appears to be conserved.

MATERIALS AND METHODS

Yeast methods

Strains used are listed in Table S1. Standard genetic techniques were used throughout (Sherman, 1991). All modifications were carried out chromosomally, except where indicated. Chromosomal tagging and deletions were performed as described previously (Knop et al., 1999; Goldstein and McCusker, 1999; Gueldener et al., 2002; Janke et al., 2004). *DCP2* and *KAP95* were genomically tagged with an auxin-inducible degron (*AID*-9MYC* and *AID*-6HA,* respectively) using pNat-AID*-9myc and pHyg-AID*-6HA plasmid templates for generation of the C-terminal tagging cassettes (Morawska and Ulrich, 2013). *NUP145* was truncated by genomic C-terminal tagging with *3MYC* to yield the mutant *nup145*ΔC allele (nucleotides 1–1815 of the original open reading frame). *TRP1* marker in the genomically integrated *YIp204-ADH1p-AFB2* was disrupted using *kanMX* or *hphMX4 cassettes.*

Plasmid construction

Shuttle vectors for expression in yeast were prepared from *pRS414-ADH* and *pRS415-GPD* backbone plasmids (Mumberg et al., 1995) by Gibson assembly using NEBuilder HiFi DNA Assembly Cloning Kit according to the manufacturer's protocol (New England Biolabs). The fragments for the assembly were prepared by PCR using Q5 High Fidelity polymerase (New England Biolabs). The plasmids used along with details on their preparation are listed in Table S2.

Fluorescence microscopy

Yeast for live-cell imaging were cultured at 30°C in YPD medium (Sherman, 1991) in case of genomically integrated modifications or in the respective HC-selection media (Burke et al., 2000) when harboring plasmids. Cultures were diluted in HC medium (Burke et al., 2000), re-grown to log phase, and either imaged directly or taken up in HC-medium and subjected to stresses (medium without glucose for 30 min or medium supplemented with 0.2 M $CaCl_2$ for 10 min). For Dcp2 depletion by auxin-inducible degron, the logarithmically growing cells before treatment with stress or imaging were treated with 2 mM auxin and cultured for 2 h.

Fluorescence and DIC images were acquired with an ORCA-flash 4.0 camera (Hamamatsu) mounted on an Axio Imager.M2 fluorescence microscope with a 63× Plan-Apochromat objective (Carl Zeiss, Germany) and a HXP 120 C light source using ZEN 2.6 software. Image processing was performed using the OMERO.insight client. For quantification of the number of foci, images from the same experiment were adjusted equally and inverted. A total of at least 300 cells from three independent experiments were quantified. Cell fluorescence measurements were carried out with ImageJ. For the nuclear-cytoplasmic GFP distribution the mean grey value of a region of interest (ROI) in the cell nucleus was normalized by the mean grey value of a ROI of the same size in the cytoplasm. A total of at least 75 cells from three independent experiments were quantified. The box and whiskers quantification graphs has the box between the 25th and the 75th percentiles, and the whiskers at the 5th and the 95th percentiles; the horizontal line marks the median and the cross indicated the mean value. The data sets were compared using a non-parametric test. *P*-values are indicated on figures. Colocalization was estimated using the JACoP plugin in ImageJ (Bolte and Cordelières, 2006). A total of at least 350 cells from three experiments were quantified.

Total protein extracts and western blot analysis

For total protein extracts 5–7 OD_{600} units of cells were spun down (2000 ***g*** for 2 min), resuspended in 200 µl 9 M urea, 50 mM Tris-HCl pH 8 with freshly added 0.5 mM PMSF and beaten 2×20 s with 0.15 ml glass beads (0.25–0.5 mm) at 6.5 m/s at 4°C. 2× Laemmli buffer (200 µl) was added and the samples were denatured at 65°C for 5 min. Samples for western blot analysis were resolved on 10 or 12.5% SDS polyacrylamide gels and transferred on Amersham Protran Premium 0.45 µm NC membrane. Membranes were decorated with the following antibodies: rabbit anti-GFP (1:5000, tp401, Torrey Pines), mouse anti-Pgk1 (22C5D8, Invitrogen, 1:2500, cat. no. 459250, Thermo Fisher Scientific), mouse anti-Por1 (16G9E6BC4, Invitrogen, 1:1000, cat. no. 459500, Thermo Fisher Scientific), rabbit anti-mCherry (1:2000, cat. no. GTX128508, GeneTex), and rabbit anti-Sec61 (1:1000, generous gift from Martin Spiess, Biozentrum Basel, Switzerland), goat anti-rabbit-IgG and anti-mouse-IgG conjugated to HRPs were from Thermo Fisher Scientific. Membranes were developed with WesternBright ECL (Advansta) at a Fusion digital imager with Evolution-capt Edge software (Vilber, France).

PolyA RNA fluorescent *in situ* hybridization

PolyA mRNA FISH was carried out in a *nup145*ΔC mutant background. *nup145*ΔC mutants are viable at 23°C, but show a strong mRNA nuclear export defect at 37°C (Kufel et al., 2004). Logarithmically growing cells, typically 10 OD_{600} units, were shifted to the non-permissive temperature (37°C) where needed, then fixed by adding formaldehyde directly to the growth medium (0.12 volumes of 37% formaldehyde containing 10–15% methanol as a stabilizer; Sigma). The samples were gently rocked for 45 min at room temperature, then washed with 4×10 ml PBS, reduced in 100 mM Tris-HCl pH 9.4, and 10 mM DTT for 10 min at room temperature and washed twice with 2 ml of ST buffer (1.4 M sorbitol, 50 mM Tris-HCl, pH 7). The cells were suspended in ST buffer (20 OD_{600} units/ml) and Zymolyase 20T was added (38 µg per OD_{600} unit), the samples were rotated at room temperature until 70–80% conversion to spheroplasts was obtained as judged by microscopy with phase contrast (typically 20–25 min). The samples were spun down (1000 ***g*** for 1 min) and carefully washed twice with 1 ml ST buffer. The cells were suspended in ST buffer (20 OD_{600} units/ml), spotted on 10-well glass slides pre-coated with 1% polyethylene imine in water, and left for 30 min at room temperature in a humidified chamber. The wells were washed with ST buffer (3×100 µl) and the slides were incubated in pre-chilled at −80°C methanol (6 min) and acetone (30 s), then briefly dried at room temperature. The wells were incubated with 50 µl 50% formamide/4× SSC for 10 min at room temperature (20× SCC is 3 M NaCl, 300 mM sodium citrate, pH 7), then with 50 µl hybridization buffer [50% formamide, 4× SSC, 0.1% Tween 20, 0.1% Triton X-100, 2× Denhardt's reagent, 0.125 mg/ml yeast tRNA (Roche) and 0.5 mg/ml salmon sperm DNA (Sigma)] for 1 h at room temperature. The wells were incubated with 30 µl 5′-Cy3-$(dT)_{30}$ probe (Microsynth, Balgach, Switzerland, 10 µg/ml in hybridization buffer) overnight at 37°C protected from light. The slides were washed at 37°C with 2× SCC (30 min), 1× SSC (30 min) and 0.5× SSC (45 min), the excess liquid was blotted off with Whatman paper, the slides were mounted in Citifluor/DAPI and sealed with nail polish.

Nuclear mRNA degradation assay

The nuclear degradation of the *MET3* mRNA was assayed in a *nup145*ΔC mutant background (see section on PolyA RNA FISH). Logarithmically growing mutant cells were first shifted to a medium lacking methionine to induce the expression of the methionine-related genes (4 h), then to 37°C for 30 min to inhibit the nuclear mRNA export and finally methionine-related gene expression was shut off by addition of excess of methionine to the medium. Aliquots were taken out, spun down and frozen in liquid nitrogen at specific times. For preparation of total RNA, the cell pellets were mixed with 300 µl 50 mM sodium acetate, pH 6, 10 mM EDTA, 25 µl 20% SDS and 300 µl phenol-chloroform-*iso*-amyl alcohol, pH 4–5. The mixtures were vortexed 30 s at top speed and incubated at 65°C for 6 min. The samples were frozen in liquid nitrogen, left to thaw for 2 min at RT and spun at 20,000 ***g*** for 10 min, 4°C. The aqueous layer was mixed with 200 µl acidic phenol-chloroform-*iso*-amyl alcohol, vortexed at top speed for 30 s and spun again. To 180 µl of the aqueous layer 20 µl 3 M sodium acetate and 600 µl ethanol was added, the mixture was chilled at −80°C for 2 h and centrifuged (20,000× ***g***, 30 min, 4°C). The pellets were washed with 400 µl 75% ethanol, spun down again, air-dried at RT, and dissolved in 30 µl water. An equal volume of 2× RNA Loading Dye (Thermo Fisher Scientific) was added, the samples were denatured at 65°C for 5 min and quickly chilled in an ice-water bath. For northern blot analysis 3–5 µg total RNA were resolved on a 1.2% agarose gel containing formaldehyde. The RNA was transferred to a Hybond N+ membrane (Amersham) and hybridized to *MET3* and *scR1* digoxigenin-labelled RNA probes. The probes were prepared by *in vitro* transcription with the MegaScript T7 kit (Ambion), Digoxigenin-11-UTP (Roche) and purified DNA templates generated by PCR. One probe covering nucleobases 20–520 was used for *scR1* and two probes covering nucleobases 5–678 and 845–1446 were used in equimolar amounts for *MET3*. Membranes were decorated with sheep anti-digoxigenin Fab fragments coupled to peroxidase (Roche). The blots were developed with WesternBright ECL (Advansta) at a Fusion digital imager with Evolution-capt Edge software (Vilber, France).

Subcellular fractionation

Logarithmically growing cells (25 OD_{600} units) were spun down (2000 ***g*** for 2 min), reduced in 100 mM Tris-HCl pH 9.4, and 10 mM DTT for 10 min and washed twice with 5 ml spheroplast buffer (0.7 M sorbitol, 0.7× YPD and 50 mM Tris-HCl pH 7.5). Cells were resuspended in spheroplast buffer (50 OD_{600} units/ml), 1 mM DTT was added and the cell wall digested with Zymolyase 20T (30 µg per OD_{600} unit) for 20 min at RT and gentle agitation. The spheroplast suspension was then layered on a 1-ml cushion of 7.5% Ficoll 400, 0.7 M sorbitol and spun at 1000 ***g*** for 2 min. The spheroplast pellet was gently resuspended in 5 ml spheroplast buffer and the spheroplasts were recovered for 1 h at RT and gentle rocking. The suspensions were spun down (1000 ***g***, 2 min), the pellets were chilled on ice and washed with 0.8 ml ice-cold lysis buffer (0.25 M sorbitol, 20 mM HEPES, pH 6.8, 5 mM $MgSO_4$ and 0.5 mM PMSF). The pellets were resuspended in lysis buffer (100 OD_{600} units/ml), sonicated twice for 45 s in a low-output cleaning bath at 4°C and spun at 2000 ***g*** for 2 min, 4°C. Typically, 0.15 ml S2 was spun at 45,000 rpm for 10 min, 4°C. The supernatant was spun at 45,000 rpm for 30 min, 4°C in a TLA 100.3 rotor (Beckman). P13, P100 and S100 were recovered, denatured with Laemmli buffer at 65°C for 5 min and analyzed by western blotting.

Polysome profiling analysis

Cycloheximide was added to the cell cultures (15 OD_{600} units) to 0.1 mg/ml final concentration from a 50 mg/ml stock in DMSO; the cultures were then swirled, chilled in an ice-water bath and shaken on ice for 10 min. The cultures were spun down (2000 ***g***, 2 min, 4°C), and the pellets were washed with 1 ml ice-cold breaking buffer (100 mM NaCl, 30 mM $MgCl_2$, 10 mM Tris-HCl pH 7.5, 0.2 mg/ml heparin and 0.1 mg/ml cycloheximide), re-suspended in 0.4 ml ice-cold breaking buffer containing RNasin Plus RNase Inhibitor (Promega, 1:1000) and 5× Halt Protease Inhibitor cocktail (Thermo Fisher Scientific), transferred to pre-chilled 2-ml screw cap tubes with 0.25 ml glass beads (0.25–0.5 mm, Roth), vortexed at top speed for 10 min at 4°C and spun down (10,000 ***g***, 3 min, 4°C). Aliquots of the clear supernatants (0.15 ml) were loaded on 5–50% linear sucrose gradients in 50 mM Tris-HCl, pH 7.5, 50 mM NH_4Cl, 12 mM $MgCl_2$. The gradients were spun at 36,000 rpm for 2 h at 4°C in a TH-641 rotor (Thermo Fisher Scientific). The gradients were formed and analyzed at a BioComp Gradient Station *ip* with continuous detection of the effluent at 260 nm.

Pulse-chase RNA labelling

Pulse-chase RNA labelling with 4-thiouracil and 4TU-labelled RNA purification was carried out as described by Wang et al. (2018).

Total RNA isolation and qRT-PCR

Total RNA isolation was carried out as for the nuclear mRNA degradation assay. The total RNA samples were treated with RQ1 RNase-free DNase (Promega) and subjected to reverse transcription with the GoScript reverse transcription mix and oligo-dT (Promega) according to the manufacturer's protocol. qRT-PCR was carried out with the Promega GoTaq qPCR Master Mix at a StepOnePlus RT-PCR system (Applied Biosystems) using *PGK1* as a reference target (Table S3). The changes in the expression levels were estimated by the $\Delta\Delta C_t$ method.

Coimmunoprecipitation

Logarithmically growing yeast cultures (12 OD_{600} units) were spun down (2000 ***g*** for 2 min), and the cell pellets were suspended in 0.6 ml ice-cold lysis buffer [100 mM NaCl, 50 mM HEPES, pH 6.8, 10 mM $MgCl_2$, 2 mM $MnCl_2$, 1 mM PMSF, 5× Halt Protease Inhibitor cocktail (Thermo Fisher Scientific)] and vortexed with 0.3 ml glass beads (0.25–0.5 mm, Roth) at top speed for 10 min at 4°C. Triton X-100 was added to 0.5% final concentration from a 10% stock, the samples were inverted several times and spun down (1000 ***g***, 2 min, 4°C). The clear supernatants (400 µl) were mixed with 20 µl RFP-Trap_MA slurry (Chromotek) and rotated for 1 h at 4°C; the beads were washed with lysis buffer with 0.5% Triton X-100, eluted with 2× Laemmli buffer at 65°C and the eluates were analyzed by western blotting.

Acknowledgements

We are grateful to thank Martin Spiess for the Sec61 antibody. We thank Rod Lim for suggesting Kap95 as the factor responsible for nuclear import for Dcp2. We acknowledge Maria Hondele and Ian G. Macara for critical comments on the manuscript.

Competing interests

The authors declare no competing or financial interests.

Author contributions

Conceptualization: K.T., A.S.; Formal analysis: K.T., A.S.; Investigation: K.T.; Writing - original draft: K.T., A.S.; Writing - review & editing: K.T., A.S.; Supervision: A.S.; Project administration: A.S.; Funding acquisition: A.S.

Funding

This work was supported by Swiss National Science Foundation (Schweizerischer Nationalfonds zur Förderung der Wissenschaftlichen Forschung; grants 310030B_163480 and 310030_185127) and the University of Basel (Universität Basel).

Peer review history

The peer review history is available online at https://journals.biologists.com/jcs/article-lookup/doi/10.1242/jcs.259156.

References

Bolte, S. and Cordelières, F. P. (2006). A guided tour into subcellular colocalization analysis in light microscopy. *J. Microsc.* **224**, 213-232. doi:10.1111/j.1365-2818.2006.01706.x

Burke, D., Dawson, D. and Stearns, T. (2000). *Methods in yeast genetics: a Cold Spring Harbor Laboratory Course Manual*. Cold Spring Harbor, New York: Cold Spring Harbor Laboratory Press.

Chang, C.-T., Bercovich, N., Loh, B., Jonas, S. and Izaurralde, E. (2014). The activation of the decapping enzyme DCP2 by DCP1 occurs on the EDC4 scaffold and involves a conserved loop in DCP1. *Nucleic Acids Res.* **42**, 5217-5233. doi:10.1093/nar/gku129

Coller, J. and Parker, R. (2005). General translational repression by activators of mRNA decapping. *Cell* **122**, 875-886. doi:10.1016/j.cell.2005.07.012

Decker, C. J., Teixeira, D. and Parker, R. (2007). Edc3p and a glutamine/asparagine-rich domain of Lsm4p function in processing body assembly in Saccharomyces cerevisiae. *J. Cell Biol.* **179**, 437-449. doi:10.1083/jcb.200704147

Decourty, L., Saveanu, C., Zemam, K., Hantraye, F., Frachon, E., Rousselle, J.-C., Fromont-Racine, M. and Jacquier, A. (2008). Linking functionally related genes by sensitive and quantitative characterization of genetic interaction profiles. *Proc. Natl. Acad. Sci. USA* **105**, 5821-5826. doi:10.1073/pnas.0710533105

Elbaz, Y. and Schuldiner, M. (2011). Staying in touch: the molecular era of organelle contact sites. *Trends Biochem. Sci.* **36**, 616-623. doi:10.1016/j.tibs.2011.08.004

Fromm, S. A., Truffault, V., Kamenz, J., Braun, J. E., Hoffmann, N. A., Izaurralde, E. and Sprangers, R. (2012). The structural basis of Edc3-and Scd6-mediated activation of the Dcp1:Dcp2 mRNA decapping complex. *EMBO J.* **31**, 279-290. doi:10.1038/emboj.2011.408

Goldstein, A. L. and Mccusker, J. H. (1999). Three new dominant drug resistance cassettes for gene disruption in Saccharomyces cerevisiae. *Yeast* **15**, 1541-1553. doi:10.1002/(SICI)1097-0061(199910)15:14<1541::AID-YEA476>3.0.CO;2-K

Gueldener, U., Heinisch, J., Koehler, G. J., Voss, D. and Hegemann, J. H. (2002). A second set of loxP marker cassettes for Cre-mediated multiple gene knockouts in budding yeast. *Nucleic Acids Res.* **30**, e23. doi:10.1093/nar/30.6.e23

Haimovich, G., Choder, M., Singer, R. H. and Trcek, T. (2013). The fate of the messenger is pre-determined: a new model for regulation of gene expression. *Biochim. Biophys. Acta (BBA) Gene Regul. Mech.* **1829**, 643-653. doi:10.1016/j.bbagrm.2013.01.004

Harigaya, Y., Jones, B. N., Muhlrad, D., Gross, J. D. and Parker, R. (2010). Identification and analysis of the interaction between Edc3 and Dcp2 in Saccharomyces cerevisiae. *Mol. Cell. Biol.* **30**, 1446-1456. doi:10.1128/MCB.01305-09

Hondele, M., Sachdev, R., Heinrich, S., Wang, J., Vallotton, P., Fontoura, B. M. A. and Weis, K. (2019). DEAD-box ATPases are global regulators of phase-separated organelles. *Nature* **573**, 144-148. doi:10.1038/s41586-019-1502-y

Janke, C., Magiera, M. M., Rathfelder, N., Taxis, C., Reber, S., Maekawa, H., Moreno-Borchart, A., Doenges, G., Schwob, E., Schiebel, E. et al. (2004). A versatile toolbox for PCR-based tagging of yeast genes: new fluorescent proteins, more markers and promoter substitution cassettes. *Yeast* **21**, 947-962. doi:10.1002/yea.1142

Kilchert, C., Weidner, J., Prescianotto-Baschong, C. and Spang, A. (2010). Defects in the secretory pathway and high Ca^{2+} induce multiple P-bodies. *Mol. Biol. Cell* **21**, 2624-2638. doi:10.1091/mbc.e10-02-0099

Knop, M., Siegers, K., Pereira, G., Zachariae, W., Winsor, B., Nasmyth, K. and Schiebel, E. (1999). Epitope tagging of yeast genes using a PCR-based strategy: more tags and improved practical routines. *Yeast* **15**, 963-972. doi:10.1002/(SICI)1097-0061(199907)15:10B<963::AID-YEA399>3.0.CO;2-W

Kornmann, B., Currie, E., Collins, S. R., Schuldiner, M., Nunnari, J., Weissman, J. S. and Walter, P. (2009). An ER-mitochondria tethering complex revealed by a synthetic biology screen. *Science* **325**, 477-481. doi:10.1126/science.1175088

Kosugi, S., Hasebe, M., Tomita, M. and Yanagawa, H. (2009). Systematic identification of cell cycle-dependent yeast nucleocytoplasmic shuttling proteins by prediction of composite motifs. *Proc. Natl. Acad. Sci. USA* **106**, 10171-10176. doi:10.1073/pnas.0900604106

Kshirsagar, M. and Parker, R. (2004). Identification of Edc3p as an enhancer of mRNA Decapping in Saccharomyces cerevisiae. *Genetics* **166**, 729-739. doi:10.1534/genetics.166.2.729

Kufel, J., Bousquet-Antonelli, C., Beggs, J. D. and Tollervey, D. (2004). Nuclear pre-mRNA decapping and 5′ degradation in yeast require the Lsm2-8p complex. *Mol. Cell. Biol.* **24**, 9646-9657. doi:10.1128/MCB.24.21.9646-9657.2004

Lee, J. E., Cathey, P. I., Wu, H., Parker, R. and Voeltz, G. K. (2020). Endoplasmic reticulum contact sites regulate the dynamics of membraneless organelles. *Science* **367**, eaay7108. doi:10.1126/science.aay7108

Luo, Y., Schofield, J. A., Simon, M. D. and Slavoff, S. A. (2020). Global profiling of cellular substrates of human Dcp2. *Biochemistry* **59**, 4176-4188. doi:10.1021/acs.biochem.0c00069

Morawska, M. and Ulrich, H. D. (2013). An expanded tool kit for the auxin-inducible degron system in budding yeast. *Yeast* **30**, 341-351. doi:10.1002/yea.2967
Mugler, C. F., Hondele, M., Heinrich, S., Sachdev, R., Vallotton, P., Koek, A. Y., Chan, L. Y. and Weis, K. (2016). ATPase activity of the DEAD-box protein Dhh1 controls processing body formation. *eLife* **5**, e18746. doi:10.7554/eLife.18746
Mumberg, D., Müller, R. and Funk, M. (1995). Yeast vectors for the controlled expression of heterologous proteins in different genetic backgrounds. *Gene* **156**, 119-122. doi:10.1016/0378-1119(95)00037-7
Nguyen Ba, A. N., Pogoutse, A., Provart, N. and Moses, A. M. (2009). NLStradamus: a simple hidden markov model for nuclear localization signal prediction. *BMC Bioinform.* **10**, 202. doi:10.1186/1471-2105-10-202
Nissan, T., Rajyaguru, P., She, M., Song, H. and Parker, R. (2010). Decapping activators in saccharomyces cerevisiae act by multiple mechanisms. *Mol. Cell* **39**, 773-783. doi:10.1016/j.molcel.2010.08.025
Paquette, D. R., Tibble, R. W., Daifuku, T. S. and Gross, J. D. (2018). Control of mRNA decapping by autoinhibition. *Nucleic Acids Res.* **46**, 6318-6329. doi:10.1093/nar/gky233
Parker, R. (2012). RNA degradation in Saccharomyces cerevisae. *Genetics* **191**, 671-702. doi:10.1534/genetics.111.137265
Prinz, W. A. (2014). Bridging the gap: membrane contact sites in signaling, metabolism, and organelle dynamics. *J. Cell Biol.* **205**, 759-769. doi:10.1083/jcb.201401126
Rajyaguru, P., She, M. and Parker, R. (2012). Scd6 targets eIF4G to repress translation: RGG motif proteins as a class of eIF4G-binding proteins. *Mol. Cell* **45**, 244-254. doi:10.1016/j.molcel.2011.11.026
Ramachandran, V., Shah, K. H. and Herman, P. K. (2011). The cAMP-dependent protein kinase signaling pathway is a key regulator of P body foci formation. *Mol. Cell* **43**, 973-981. doi:10.1016/j.molcel.2011.06.032
Rao, B. S. and Parker, R. (2017). Numerous interactions act redundantly to assemble a tunable size of P bodies in Saccharomyces cerevisiae. *Proc. Natl. Acad. Sci. USA* **114**, E9569-E9578. doi:10.1073/pnas.1712396114
Sachdev, R., Hondele, M., Linsenmeier, M., Vallotton, P., Mugler, C. F., Arosio, P. and Weis, K. (2019). Pat1 promotes processing body assembly by enhancing the phase separation of the DEAD-box ATPase Dhh1 and RNA. *eLife* **8**, e41415. doi:10.7554/eLife.41415
Sharif, H., Ozgur, S., Sharma, K., Basquin, C., Urlaub, H. and Conti, E. (2013). Structural analysis of the yeast Dhh1-Pat1 complex reveals how Dhh1 engages Pat1, Edc3 and RNA in mutually exclusive interactions. *Nucleic Acids Res.* **41**, 8377-8390. doi:10.1093/nar/gkt600
Sherman, F. (1991). Getting started with yeast. *Methods Enzymol.* **194**, 3-21. doi:10.1016/0076-6879(91)94004-V
Sheth, U. and Parker, R. (2003). Decapping and decay of messenger RNA occur in cytoplasmic processing bodies. *Science* **300**, 805-808. doi:10.1126/science.1082320
Teixeira, D. and Parker, R. (2007). Analysis of P-body assembly in Saccharomyces cerevisiae. *Mol. Biol. Cell* **18**, 2274-2287. doi:10.1091/mbc.e07-03-0199
Tesina, P., Heckel, E., Cheng, J., Fromont-Racine, M., Buschauer, R., Kater, L., Beatrix, B., Berninghausen, O., Jacquier, A., Becker, T. et al. (2019). Structure of the 80S ribosome–Xrn1 nuclease complex. *Nat. Struct. Mol. Biol.* **26**, 275-280. doi:10.1038/s41594-019-0202-5
Van Dijk, E., Cougot, N., Meyer, S., Babajko, S., Wahle, E. and Séraphin, B. (2002). Human Dcp2: a catalytically active mRNA decapping enzyme located in specific cytoplasmic structures. *EMBO J.* **21**, 6915-6924. doi:10.1093/emboj/cdf678
Vindry, C., Marnef, A., Broomhead, H., Twyffels, L., Ozgur, S., Stoecklin, G., Llorian, M., Smith, C. W., Mata, J., Weil, D. et al. (2017). Dual RNA processing roles of Pat1b via cytoplasmic Lsm1-7 and nuclear Lsm2-8 complexes. *Cell Rep.* **20**, 1187-1200. doi:10.1016/j.celrep.2017.06.091
Wang, C., Schmich, F., Srivatsa, S., Weidner, J., Beerenwinkel, N. and Spang, A. (2018). Context-dependent deposition and regulation of mRNAs in P-bodies. *eLife* **7**, e29815. doi:10.7554/eLife.29815
Weidner, J., Wang, C., Prescianotto-Baschong, C., Estrada, A. F. and Spang, A. (2014). The polysome-associated proteins Scp160 and Bfr1 prevent P body formation under normal growth conditions. *J. Cell Sci.* **127**, 1992-2004. doi:10.1242/jcs.142083
Xing, W., Muhlrad, D., Parker, R. and Rosen, M. K. (2020). A quantitative inventory of yeast P body proteins reveals principles of composition and specificity. *eLife* **9**, e56525. doi:10.7554/eLife.56525
Yoon, J.-H., Choi, E.-J. and Parker, R. (2010). Dcp2 phosphorylation by Ste20 modulates stress granule assembly and mRNA decay in Saccharomyces cerevisiae. *J. Cell Biol.* **189**, 813-827. doi:10.1083/jcb.200912019
Zeidan, Q., He, F., Zhang, F., Zhang, H., Jacobson, A. and Hinnebusch, A. G. (2018). Conserved mRNA-granule component Scd6 targets Dhh1 to repress translation initiation and activates Dcp2-mediated mRNA decay in vivo. *PLoS Genet.* **14**, e1007806. doi:10.1371/journal.pgen.1007806

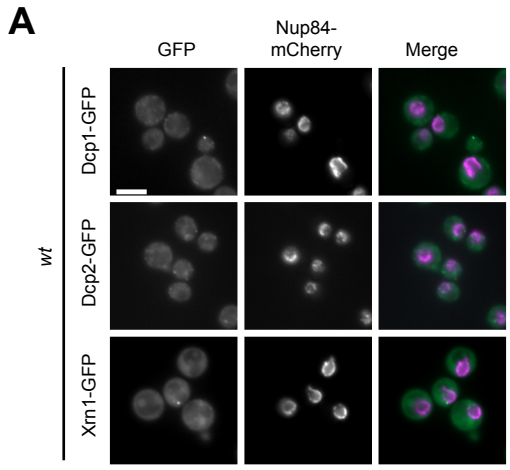

Fig. S1. Concomitant loss of Scd6 and Edc3 blocks P-body assembly and drives nuclear accumulation of Dcp2. (A) Wild-type control strains show no nuclear enrichment of either the decapping complex components Dcp1 and Dcp2, or the exonuclease Xrn1. Logarithmically growing cells expressing genomically tagged Dcp1-, Dcp2- or Xrn1-GFP and the nuclear marker Nup84-mCherry were imaged without additional treatment. Scale bar 5 μm.

A

NLStradamus prediction results for Dcp2

NLS Designation	Sequence
K450	^{450}KKPDSNVQSSKKPKLKIL^{467}
S564	^{564}SRRSQKEKPRN^{574}
K697	^{697}KKVPKVKILKRGE^{709}

Four state HMM static prediction with cut off 0.2

B

cNLS cutter prediction results for Dcp2

Bipartite NLS sequence	Score
^{75}IIKLCPLVWKWDIRVDEALQQFSKYKKSI	4.0
^{75}IIKLCPLVWKWDIRVDEALQQFSKYKKSIP	3.2
^{216}KSNIKYYLINSMMRPLSMWLRHQRQIKNED	3.8
^{673}RDMPTESNKSINETVGLSSTTNTVKKVPKVKILKR	6.7
^{730}SKDLLQMLRNPISSTVSSNQQSPKSQHLS	4.1
^{805}DITAPKQPYNVDSYSQKNSAKGLLNILKKNDST	3.6
^{831}LKKNDSTGYPRTEGGPSSEMSTSMKRNDAT	3.7
^{852}TSMKRNDATNNQELDKNSTELLNYLKPKP	3.0
^{852}TSMKRNDATNNQELDKNSTELLNYLKPKPL	3.3

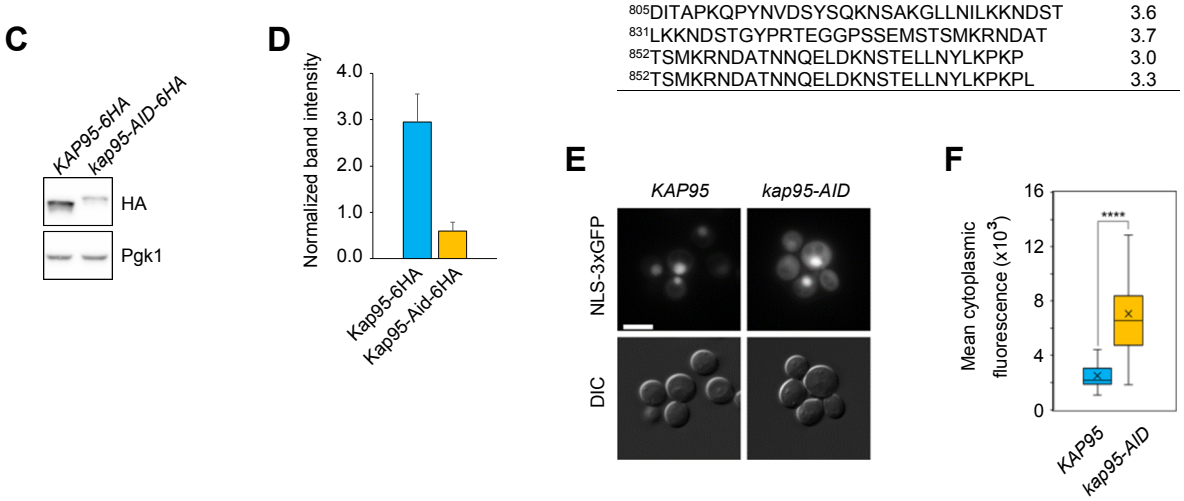

Fig. S2. Dcp2 uses two distinct NLSs and Kap95 for nuclear localization. (A) and (B) Putative NLSs identified in the *Sc* Dcp2 protein sequence using NLStradamus and cNLS cutter web-based tools. (C) and (D) Kap95 C-terminal tagging with an auxin-inducible degron reduces its steady-state levels. Steady-state levels of Kap95 tagged genomically either with 6HA or 6HA-Aid were determined in total protein lysates of logarithmically growing cells by Western blotting using Pgk1 as a reference. (E) and (F) *KAP95* genomic tagging with an auxin-inducible degron results in a defect in the nuclear import of canonical NLSs. (E) Logarithmically growing cells expressing 3xGFP bearing an N-terminal SV40 NLS from a strong promoter (*GPDp*) were imaged without further treatment. Scale bar 5 μm. (F) Quantification of the mean cytoplasmic fluorescence intensity of the cells in panel E.

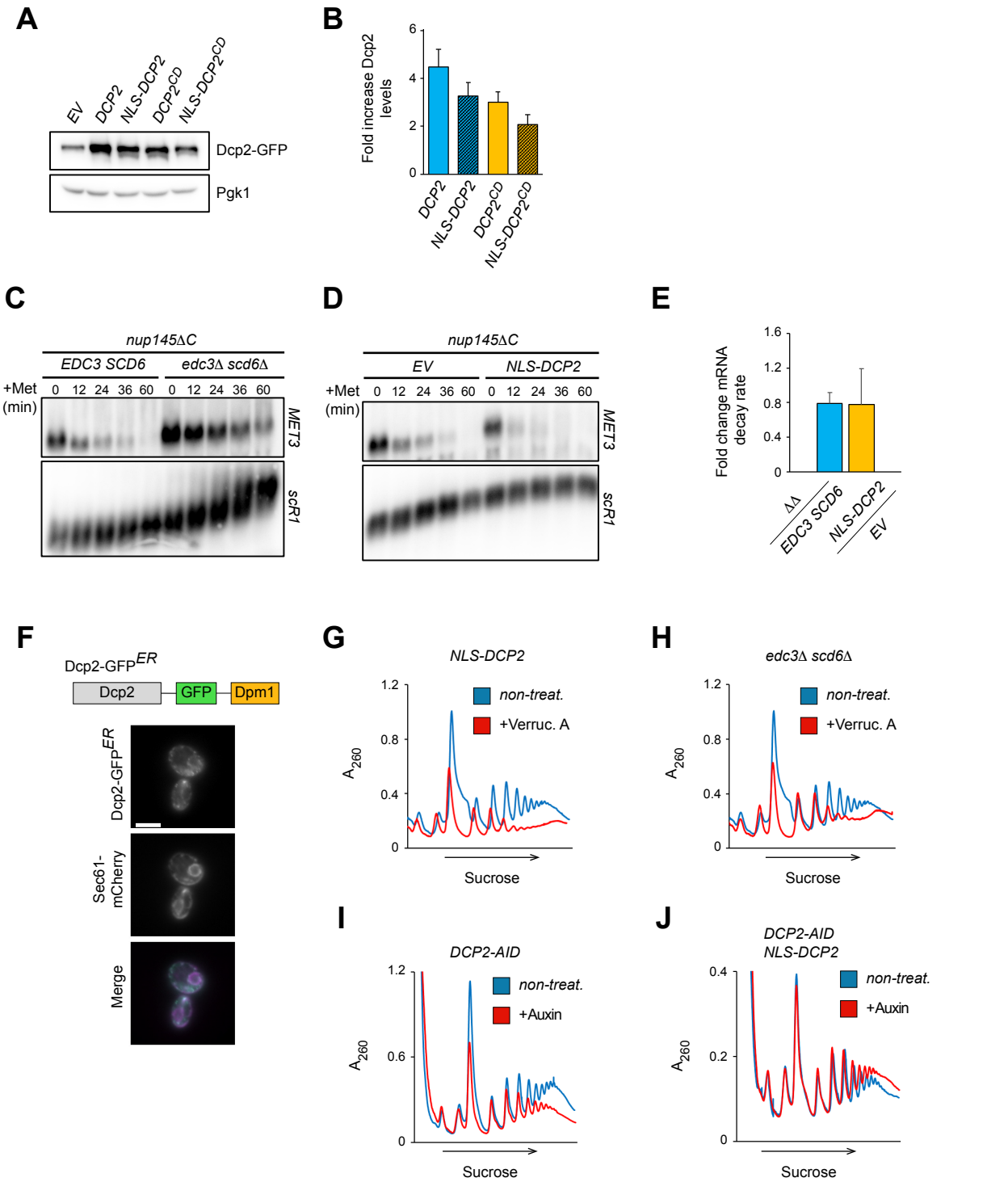
A
EV
DCP2
NLS-DCP2
DCP2CD
NLS-DCP2CD
Dcp2-GFP
Pgk1
B
Fold increase Dcp2 levels
6
4
2
0
DCP2
NLS-DCP2
DCP2CD
NLS-DCP2CD
C
nup145ΔC
EDC3 SCD6
edc3Δ scd6Δ
+Met
(min)
0 12 24 36 60 0 12 24 36 60
MET3
scR1
D
nup145ΔC
EV
NLS-DCP2
+Met
(min)
0 12 24 36 60 0 12 24 36 60
MET3
scR1
E
Fold change mRNA decay rate
1.6
1.2
0.8
0.4
0
ΔΔ
EDC3 SCD6
NLS-DCP2
EV
F
Dcp2-GFPER
Dcp2
GFP
Dpm1
Dcp2-GFPER
Sec61-mCherry
Merge
G
NLS-DCP2
non-treat.
+Verruc. A
A260
1.2
0.8
0.4
0
Sucrose
H
edc3Δ scd6Δ
non-treat.
+Verruc. A
A260
1.2
0.8
0.4
0
Sucrose
I
DCP2-AID
non-treat.
+Auxin
A260
1.2
0.6
0
Sucrose
J
DCP2-AID
NLS-DCP2
non-treat.
+Auxin
A260
0.4
0.2
0
Sucrose

Fig. S3. The decapping complex is stored in the nucleus as a readily releasable pool. (A) and (B) Overexpression of NLS-appended and catalytically dead (CD) variants of Dcp2. Cells expressing Dcp2-GFP from a genomic locus were transformed with a low-copy plasmid expressing different versions of Dcp2-GFP from the strong *GPD* promoter. The GFP expression of logarithmically growing cells was analyzed by Western blotting and quantified using Pgk1 as reference. (C)-(E) Northern blot analysis of *MET3* mRNA nuclear degradation. *nup145*ΔC strain background was either deleted for *EDC3* and *SCD6* or transformed with low-copy plasmids expressing the indicated Dcp2 constructs. Logarithmically growing cultures were starved for methionine to induce the expression of *MET3* and then shifted to 37°C to inhibit mRNA nuclear export. *MET3* transcription was then blocked by addition of methionine and aliquots for Northern blotting analysis were taken at the indicated time points. The *scR1* mRNA served as a loading control. (F) ER-localization of the Dcp2-GFP-Dpm1 construct. Cells expressing the ER-marker Sec61-mCherry were transformed with the low-copy construct expressing Dcp2-GFP-Dpm1 from the *DCP2* promoter. Logarithmically growing cultures were imaged without treatment. Scale bar 5 μm. (G) and (H) Translation attenuation upon treatment with verrucarin A. The global translation in wild-type cells expressing NLS-Dcp2-GFP from a strong promoter or *edc3*Δ *scd6*Δ expressing genomically tagged Dcp2-GFP was analyzed by polysome profiling upon verrucarin A treatment as in Figure 3-I. (I) and (J) NLS-Dcp2 rescues translation upon depletion of the endogenous Dcp2. Cells with *DCP2* tagged genomically with an auxin-inducible degron were transformed with a low-copy plasmid expressing NLS-Dcp2 from a *GPD* promoter. The global translation of logarithmically growing cultures was analyzed by polysome profiling upon depletion of the endogenous Dcp2 with auxin.

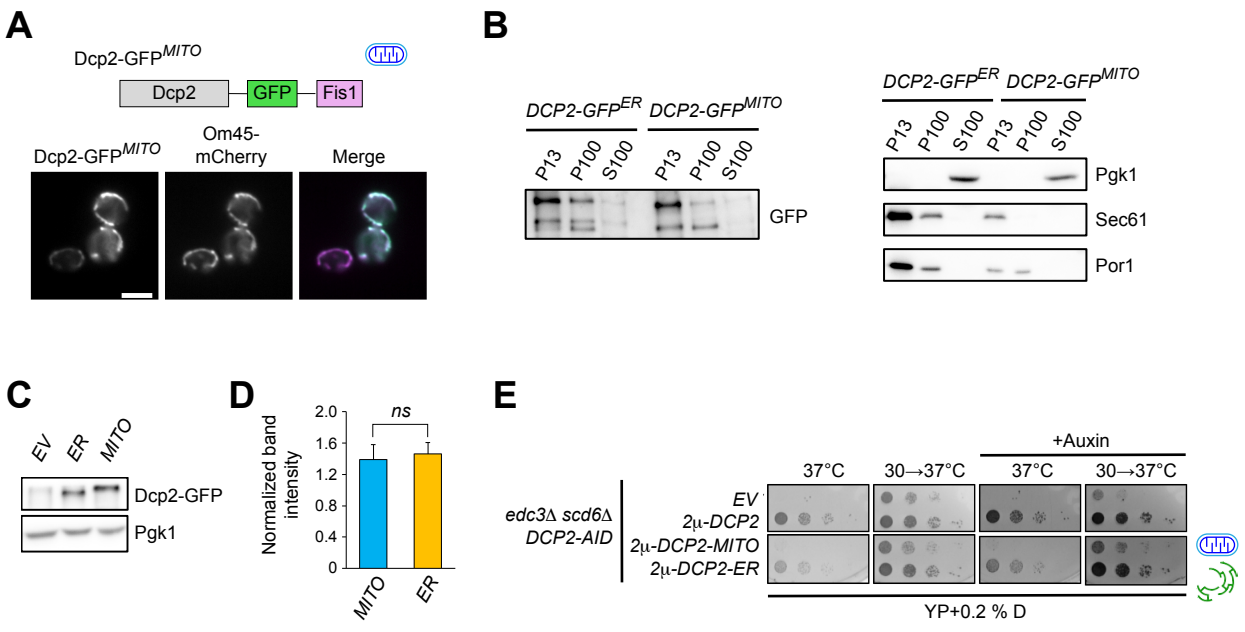

Fig. S4. Dcp1/Dcp2 performs essential functions on the cytoplasmic face of the ER. (A) and (B) Subcellular localization of the Dcp2-GFP^{MITO} and Dcp2-GFP^{ER}. *edc3*Δ *scd6*Δ with genomically tagged Om45-mCherry were transformed with a low-copy plasmid expressing Dcp2-GFP-Fis1 (Dcp2-GFP^{MITO}) from a *DCP2* promoter. Logarithmically growing cultures were imaged directly, scale bar 5 μm (A). (B) Subcellular localization of Dcp2-GFP^{ER} and Dcp2-GFP^{MITO}. *edc3*Δ *scd6*Δ with *DCP2* tagged genomically with an auxin-inducible degron were transformed with low-copy plasmids expressing the Dcp2-GFP-Dpm1 (Dcp2-GFP^{ER}) or Dcp2-GFP-Fis1 (Dcp2-GFP^{MITO}) from the endogenous *DCP2* promoter. Spheroplast lysates were subjected to differential centrifugation and the P13, P100 and S100 fractions analyzed by Western blotting. (C) and (D) Dcp2-GFP^{ER} and Dcp2-GFP^{MITO} are expressed at similar levels. The Dcp2-GFP levels in logarithmically growing cells from the strains in panel B and an empty vector control were analyzed by Western blotting. (E) Dcp2 at the ER is required for growth under stress. *edc3*Δ *scd6*Δ with *DCP2* tagged genomically with an auxin-inducible degron were transformed with high-copy plasmids expressing the indicated Dcp2-constructs from the endogenous *DCP2* promoter. Serial dilutions of the respective logarithmically growing cultures were spotted on YP-agar with 0.2 % glucose, supplemented with 0.2 M auxin as indicated. Agar plates were incubated for 2 days at 37°C, and followed by 3 days at 30°C. (F) and (G) Dcp2-GFP^{MITO} is able to recruit other PB components. Strains with *DCP2* tagged genomically with an auxin-inducible degron were transformed with low-copy plasmids expressing Pat1-mCherry, resp. Dhh1-mCherry from its own promoter. Logarithmically growing cells were treated with 2 mM auxin for 2 h, then subjected to 30 min glucose deprivation and imaged. Scale bar 5 μm. (H) and (I) Dcp2-GFP^{MITO} levels do not change upon deletion of *MMM1*. *edc3*Δ *scd6*Δ *DCP2-AID* was deleted for *MMM1* and the Dcp2-GFP^{MITO} levels expressed from a low-copy plasmid on the *DCP2* promoter were determined by Western blotting and compared with isogenic background strain.

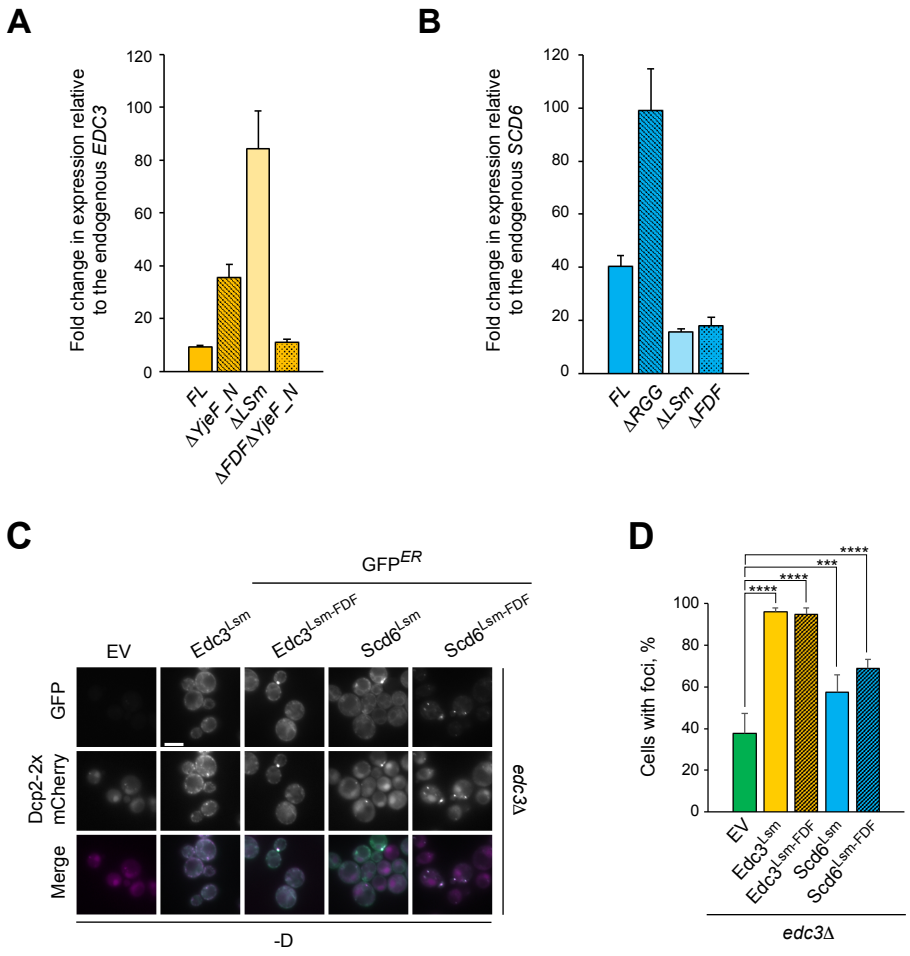

Fig. S5. Scd6 and Edc3 bridge the interaction of Dcp2 with Dhh1 during P-body assembly. (A) and (B) Expression of the *EDC3* and *SCD6* domain constructs. Wild-type or *edc3*Δ *scd6*Δ with genomically tagged Dcp2-GFP were transformed with low-copy plasmids expressing the indicated *SCD6* or *EDC3* constructs from the strong *GPD* promoter. Logarithmically growing cells were harvested and levels of the respective construct mRNAs relative to PGK1 were determined by qRT-PCR. (C) Bridging Dcp2 to Dhh1 at the ER rescues PB-formation in *edc3*Δ. *edc3*Δ cells with *DCP2* genomically tagged with 2×mCherry were transformed with low-copy constructs expressing GFP-ER-anchored (as fusions with Dpm1) Edc3 and Scd6 truncations from the respective own promoters. Logarithmically growing cultures were starved for glucose for 30 min and imaged. (D) Quantification of the number of Dcp2-2×mCherry foci in the strains from panel C upon 30 min –D.

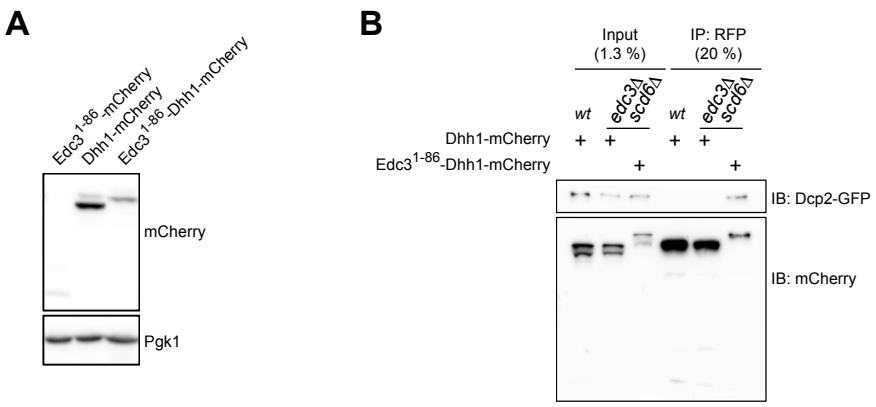

Fig. S6. Linking Dcp2 and Dhh1 drives P-body formation and functional stress response. (A) The Edc3$^{1\text{-}86}$-Dhh1 fusion is expressed at lower levels than Dhh1. The expression of the mCherry constructs from Figure 6-A in an *edc3*Δ *scd6*Δ background was analyzed by Western blotting. (B) The Edc3 LSm-domain (Edc3$^{1\text{-}86}$) efficiently links Dhh1 to Dcp2. Logarithmically growing wild-type or *edc3*Δ *scd6*Δ cells expressing the indicated constructs from a low-copy vector and the *DHH1* promoter were immunoprecipitated with RFP_Trap and the immunoprecipitates were analyzed by Western blotting.

Table S1. *S. cerevisiae* strains used in the study

Strain	Genotype	Reference
YPH499	*MAT a ade2-101 his3-200 leu2-1 lys2-801 trp-63 ura3-52*	(Sikorski and Hieter, 1989)
YAS1031A	*MATa ade2::ARF1::ADE2 arf1::HIS3 arf2::HIS3 ura3 lys2 trp1 his3 leu2 DCP2::DCP2-yEGFP-kanMX4*	(Kilchert *et al.*, 2010)
YAS1097	*MATa ade2::ARF1::ADE2 arf1::HIS3 arf2::HIS3 ura3 lys2 trp1 his3 leu2 DCP2::DCP2-yEGFP-kanMX4 scd6Δ::LEU2 (K.lactis)*	(Kilchert *et al.*, 2010)
YAS2300	*MATa ade2::ARF1::ADE2 arf1::HIS3 arf2::HIS3 ura3 lys2 trp1 his3 leu2 DCP2::DCP2-yEGFP-kanMX4 edc3Δ::URA3 (K.lactis)*	(Kilchert, 2010)
YAS5243	*MATa ade2::ARF1::ADE2 arf1::HIS3 arf2::HIS3 ura3 lys2 trp1 his3 leu2 DCP2::DCP2-yEGFP-kanMX4 edc3Δ::URA3 (K.lactis) scd6Δ::natMX4*	This study
YAS5716	*MATa ade2::ARF1::ADE2 arf1::HIS3 arf2::HIS3 ura3 lys2 trp1 his3 leu2 DCP1::DCP1-yEGFP-hphNT1 NUP84::NUP84-mCherry-natNT1*	This study
YAS5281	*MATa ade2::ARF1::ADE2 arf1::HIS3 arf2::HIS3 ura3 lys2 trp1 his3 leu2 DCP2::DCP2-yEGFP-kanMX4 NUP84::NUP84-mCherry-natNT1*	This study
YAS5718	*MATa ade2::ARF1::ADE2 arf1::HIS3 arf2::HIS3 ura3 lys2 trp1 his3 leu2 XRN1::XRN1-yEGFP-TRP1 (K.lactis) NUP84::NUP84-mCherry-natNT1*	This study
YAS5278	*MATa ade2::ARF1::ADE2 arf1::HIS3 arf2::HIS3 ura3 lys2 trp1 his3 leu2 DCP1::DCP1-yEGFP-kanMX4 NUP84::NUP84-mCherry-natNT1 edc3::URA3 (K.lactis) scd6::LEU2 (K.lactis)*	This study
YAS5311	*MATa ade2::ARF1::ADE2 arf1::HIS3 arf2::HIS3 ura3 lys2 trp1 his3 leu2 DCP2::DCP2-yEGFP-kanMX4 NUP84::NUP84-mCherry-natNT1 edc3Δ::URA3 (K.lactis) scd6Δ::LEU (K.lactis)*	This study
YAS5313	*MATa ade2::ARF1::ADE2 arf1::HIS3 arf2::HIS3 ura3 lys2 trp1 his3 leu2 XRN1::XRN1-yEGFP-TRP1 (K.lactis) NUP84::NUP84-mCherry-natNT1 edc3Δ::URA3 (K.lactis) scd6Δ::LEU2 (K.lactis)*	This study
YAS2355	*MATa ade2::ARF1::ADE2 arf1::HIS3 arf2::HIS3 ura3 lys2 trp1 his3 leu2 DCP2::DCP2-yEGFP-kanMX4 lsm1Δ::URA3 (K.lactis)*	(Kilchert, 2010)
YAS5314	*MATa ade2::ARF1::ADE2 arf1::HIS3 arf2::HIS3 ura3 lys2 trp1 his3 leu2 DCP2::DCP2-yEGFP-kanMX4 edc3Δ::URA3 (K.lactis) scd6Δ::natMX4 dcp1Δ::LEU2 (K.lactis)*	This study
YAS5871	*MATa ade2::ARF1::ADE2 arf1::HIS3 arf2::HIS3 ura3 lys2 trp1 his3 leu2 NUP84::NUP84-mCherry-natNT1 edc3Δ::URA3 (K.lactis) scd6Δ::hphMX4*	This study
YAS2298	*MATa ade2::ARF1::ADE2 arf1::HIS3 arf2::HIS3 ura3 lys2 trp1 his3 leu2 edc3Δ::URA3 (K.lactis)*	(Kilchert, 2010)
YAS5890	*MATa ade2::ARF1::ADE2 arf1::HIS3 arf2::HIS3 ura3 lys2 trp1 his3 leu2 KAP95::kap95-aid-6HA-hph edc3Δ::URA3 (K.lactis)*	This study
YAS5996	*MATa ade2::ARF1::ADE2 arf1::HIS3 arf2::HIS3 ura3 lys2 trp1 his3 leu2 DCP2::DCP2-yEGFP-kanMX4 NUP84::NUP84-mCherry-natNT1 KAP95::kap95-aid-6HA-hph edc3Δ::URA3 (K.lactis) scd6Δ::LEU2 (K.lactis)*	This study
YAS5788	*MATa ade2::ARF1::ADE2 arf1::HIS3 arf2::HIS3 ura3 lys2 trp1 his3 leu2 DCP2::DCP2-yEGFP-kanMX4 NUP84::NUP84-mCherry-natNT1 KAP95::KAP95-6HA-TRP1 edc3Δ::URA3 (K.lactis) scd6Δ::LEU2 (K.lactis)*	This study
YAS5391	*MATa ade2::ARF1::ADE2 arf1::HIS3 arf2::HIS3 ura3 lys2 trp1 his3 leu2 DCP2::DCP2-yEGFP-kanMX4 NUP145::nup145ΔC-3MYC-TRP1*	This study
YAS5392	*MATa ade2::ARF1::ADE2 arf1::HIS3 arf2::HIS3 ura3 lys2 trp1 his3 leu2 DCP2::DCP2-yEGFP-kanMX4 NUP145::nup145ΔC-3MYC-TRP1 edc3Δ::URA3 (K.lactis) scd6Δ::natMX4*	This study
YAS5905	*MATa ade2::ARF1::ADE2 arf1::HIS3 arf2::HIS3 ura3 lys2 trp1 his3 leu2 SEC61::SEC61-mCherry-kanMX4*	This study
YAS4163	*MATa ade2::ARF1::ADE2 arf1::HIS3 arf2::HIS3 ura3 lys2 trp1 his3 leu2 DCP2::DCP2-2xmCherry-hphNT1*	(Wang *et al.*, 2018)
YAS5888	*MATa ade2::ARF1::ADE2 arf1::HIS3 arf2::HIS3 ura3 lys2 trp1 his3 leu2 DCP2::DCP2-2xmCherry-hphNT1 edc3Δ::natMX4*	This study
YAS5449	*MATa ade2::ARF1::ADE2 arf1::HIS3 arf2::HIS3 ura3 lys2 trp1 his3 leu2 DCP2::DCP2-AID-9MYC-natNT trp1::ADHp-AFB2-TRP1*	This study

YAS5639	*MATa ade2::ARF1::ADE2 arf1::HIS3 arf2::HIS3 ura3 lys2 trp1 his3 leu2 DCP2::DCP2-AID-9MYC-natNT trp1::ADHp-AFB2-TRP1 trp1Δ::kanMX4*	This study
YAS5483	*MATa ade2::ARF1::ADE2 arf1::HIS3 arf2::HIS3 ura3 lys2 trp1 his3 leu2 DCP2::DCP2-AID-9MYC-natNT trp1::ADHp-AFB2-TRP1 edc3Δ::URA3 (K.lactis) scd6Δ::LEU2 (K.lactis)*	This study
YAS5641	*MATa ade2::ARF1::ADE2 arf1::HIS3 arf2::HIS3 ura3 lys2 trp1 his3 leu2 DCP2::DCP2-AID-9MYC-natNT trp1::ADHp-AFB2-TRP1 edc3Δ::URA3 (K.lactis) scd6Δ::hphMX4 trp1Δ::kanMX4*	This study
YAS5644	*MATa ade2::ARF1::ADE2 arf1::HIS3 arf2::HIS3 ura3 lys2 trp1 his3 leu2 DCP2::DCP2-AID-9MYC-natNT MDM34::MDM34-mCherry-kanMX4 trp1::ADHp-AFB2-TRP1 edc3Δ::URA3 (K.lactis) scd6Δ::LEU2 (K.lactis) trp1Δ::hphMX4*	This study
YAS5721	*MATa ade2::ARF1::ADE2 arf1::HIS3 arf2::HIS3 ura3 lys2 trp1 his3 leu2 DCP2::DCP2-AID-9MYC-natNT OM45::OM45-mCherry-kanMX4 trp1::ADHp-AFB2-TRP1 edc3Δ::URA3 (K.lactis) scd6Δ::LEU2 (K.lactis) trp1Δ::hphMX4*	This study
YAS5713	*MATa ade2::ARF1::ADE2 arf1::HIS3 arf2::HIS3 ura3 lys2 trp1 his3 leu2 DCP2::DCP2-AID-9MYC-natNT trp1::ADHp-AFB2-TRP1 edc3Δ::URA3 (K.lactis) mmm1Δ::LEU2 (K.lactis) scd6Δ::hphMX4 trp1Δ::kanMX4*	This study
YAS5705	*MATa ade2::ARF1::ADE2 arf1::HIS3 arf2::HIS3 ura3 lys2 trp1 his3 leu2 DCP2::DCP2-AID-9MYC-natNT XRN1::XRN1-mCherry-kanMX4 trp1::ADHp-AFB2-TRP1*	This study
YAS5707	*MATa ade2::ARF1::ADE2 arf1::HIS3 arf2::HIS3 ura3 lys2 trp1 his3 leu2 DCP2::DCP2-AID-9MYC-natNT EDC3::EDC3-yEGFP-hphNT1 XRN1::XRN1-mCherry-kanMX4 trp1::ADHp-AFB2-TRP1*	This study
YAS5709	*MATa ade2::ARF1::ADE2 arf1::HIS3 arf2::HIS3 ura3 lys2 trp1 his3 leu2 DCP2::DCP2-AID-9MYC-natNT SCD6::SCD6-yEGFP-hphNT1 trp1::ADHp-AFB2-TRP1*	This study

Table S2. Yeast plasmids used in the study

Construct	Primers and templates for PCR generation of the assembly fragments				Vector	Vector cut with
	Fragment	Primer	Primer sequence	PCR template		
pRS414-PAT1p-PAT1-mCherry	*PAT1p-PAT1*	kt2026	AGGGAACAAAAGCTGGAGCTGAGGGTTCAGGGAAATCC	gDNA YPH499	*pRS414-ADHp*	*Sac*I/*Sal*I
		kt2101	GTCGACCTGCAGCGTACG CTTTAGTTCTGATATTTCACC			
	mCherry	kt2103	CGT ACG CTG CAG GTC GAC	*pYM-mCherry-kanMX*		
		kt2070a	TACCGGGCCCCCCCCTCGAGGTCGAC ATGGGGATGTATGGGCTAAA			
pRS415-PAT1p-PAT1-mCherry	*PAT1p-PAT1*	kt2026	AGGGAACAAAAGCTGGAGCTGAGGGTTCAGGGAAATCC	gDNA YPH499	*pRS415-GPDp*	*Sac*I/*Sal*I
		kt2101	GTCGACCTGCAGCGTACG CTTTAGTTCTGATATTTCACC			
	mCherry	kt2103	CGT ACG CTG CAG GTC GAC	*pYM-mCherry-kanMX*		
		kt2070a	TACCGGGCCCCCCCCTCGAGGTCGAC ATGGGGATGTATGGGCTAAA			
pRS415-GPDp-DCP2-GFP	*DCP2*	kt2066	CGGCCGCTCTAGAACTAGTGGATCCATGTCACTGCCGCTACGACAC	gDNA YPH499	*pRS415-GPDp*	*Bam*HI/*Xho*I
		kt2068	GTCGACCTGCAGCGTACGCTTCCTATGCAAAATGCTTAA			
	GFP	kt2069	TTAAGCATTTTGCATAGGAAG CGT ACG CTG CAG GTC GAC	*pYM44*		
		kt2070	GGTACCGGGCCCCCCCTCGAG ATGGGGATGTATGGGCTAAA			
pRS415-GPDp-NLS-DCP2-GFP	*NLS-DCP2*	kt2076	CGGCCGCTCTAGAACTAGTGGATCCATG CCA AAG AAG AAA AGA AAG GTT TCACTGCCGCTACGACAC	gDNA YPH499	*pRS415-GPDp*	*Bam*HI/*Xho*I
		kt2068	GTCGACCTGCAGCGTACGCTTCCTATGCAAAATGCTTAA			
	GFP	kt2069	TTAAGCATTTTGCATAGGAAG CGT ACG CTG CAG GTC GAC	*pYM44*		
		kt2070	GGTACCGGGCCCCCCCTCGAG ATGGGGATGTATGGGCTAAA			
pRS415-GPDp-DCP2(cat. dead)-GFP	*DCP2p-DCP2-mut-1*	kt2066	CGGCCGCTCTAGAACTAGTGGATCCATGTCACTGCCGCTACGACAC	gDNA YPH499	*pRS415-GPDp*	*Bam*HI/*Xho*I
		kt2077	ACCAAT TGCAGCTTTAACTGCAGC AATGCAACAATCTATGTCATT			
	DCP2-mut-2	kt2078	TGCATT GCT GCA GTT AAA GCT GCA ATTGGTTTCGATTTGACGGAC	gDNA YPH499		
		kt2068	GTCGACCTGCAGCGTACGCTTCCTATGCAAAATGCTTAA			
	GFP	kt2069	TTAAGCATTTTGCATAGGAAG CGT ACG CTG CAG GTC GAC	*pYM44*		
		kt2070	GGTACCGGGCCCCCCCTCGAG ATGGGGATGTATGGGCTAAA			
pRS415-GPDp-NLS-DCP2(cat. dead)-GFP	*NLS-DCP2-mut-1*	kt2076	CGGCCGCTCTAGAACTAGTGGATCCATG CCA AAG AAG AAA AGA AAG GTT TCACTGCCGCTACGACAC	gDNA YPH499	*pRS415-GPDp*	*Bam*HI/*Xho*I
		kt2077	ACCAAT TGCAGCTTTAACTGCAGC AATGCAACAATCTATGTCATT			
	DCP2-mut-2	kt2078	TGCATT GCT GCA GTT AAA GCT GCA ATTGGTTTCGATTTGACGGAC	gDNA YPH499		
		kt2068	GTCGACCTGCAGCGTACGCTTCCTATGCAAAATGCTTAA			
	GFP	kt2069	TTAAGCATTTTGCATAGGAAG CGT ACG CTG CAG GTC GAC	*pYM44*		
		kt2070	GGTACCGGGCCCCCCCTCGAG ATGGGGATGTATGGGCTAAA			
pRS414-DCP2p-DCP2-GFP-FIS1	*DCP2p-DCP2*	kt2072	AGGGAACAAAAGCTGGAGCTC ATAATAAGGGTCATCGATCC	gDNA YPH499	*pRS414-ADHp*	*Sac*I/*Sal*I
		kt2068	GTCGACCTGCAGCGTACGCTTCCTATGCAAAATGCTTAA			
	GFP	kt2069	TTAAGCATTTTGCATAGGAAG CGT ACG CTG CAG GTC GAC	*pYM44*		
		kt2073	TTCGCCGCTGCCCGCGGCAGCGCGGGCAGC TTTGTACAATTCATCCAT			
	FIS1	kt2074	TTGTACAAA GCTGCCCGCGCTGCCGCGGGCAGCGGCGAA ATGACCAAAGTAGATTTT	gDNA YPH499		
		kt2075	TACCGGGCCCCCCCTCGAGGTCGAC AGAAGGCAAAATAGCAGTG			

Table S2 (continued)

pRS414-DCP2p-DCP2-GFP-DPM1	*DCP2p-DCP2*	kt2072	AGGGAACAAAAGCTGGAGCTC ATAATAAGGGTCATCGATCC	gDNA YPH499	*pRS414-ADHp*	*Sac*I/*Sal*I
		kt2068	GTCGACCTGCAGCGTACGCTTCCTATGCAAAATGCTTAA			
	GFP	kt2069	TTAAGCATTTTGCATAGGAAG CGT ACG CTG CAG GTC GAC	*pYM44*		
		kt2073	TTCGCCGCTGCCCGCGGCAGCGCGGGCAGC TTTGTACAATTCATCCAT			
	DPM1	kt2081	TTGTACAAA GCTGCCCGCGCTGCCGCGGGCAGCGGCGAA ATGAGCATCGAATACTCTGT	gDNA YPH499		
		kt2082	TACCGGGCCCCCCCTCGAGGTCGAC TAATGATCTATTCATAAAGCA			
pRS424-DCP2p-DCP2-GFP-FIS1	*DCP2p-DCP2*	kt2072	AGGGAACAAAAGCTGGAGCTC ATAATAAGGGTCATCGATCC	gDNA YPH499	*pRS424-ADHp*	*Sac*I/*Sal*I
		kt2068	GTCGACCTGCAGCGTACGCTTCCTATGCAAAATGCTTAA			
	GFP	kt2069	TTAAGCATTTTGCATAGGAAG CGT ACG CTG CAG GTC GAC	*pYM44*		
		kt2073	TTCGCCGCTGCCCGCGGCAGCGCGGGCAGC TTTGTACAATTCATCCAT			
	FIS1	kt2074	TTGTACAAA GCTGCCCGCGCTGCCGCGGGCAGCGGCGAA ATGACCAAAGTAGATTTT	gDNA YPH499		
		kt2075	TACCGGGCCCCCCCTCGAGGTCGAC AGAAGGCAAAATAGCAGTG			
pRS424-DCP2p-DCP2-GFP-DPM1	*DCP2p-DCP2*	kt2072	AGGGAACAAAAGCTGGAGCTC ATAATAAGGGTCATCGATCC	gDNA YPH499	*pRS424-ADHp*	*Sac*I/*Sal*I
		kt2068	GTCGACCTGCAGCGTACGCTTCCTATGCAAAATGCTTAA			
	GFP	kt2069	TTAAGCATTTTGCATAGGAAG CGT ACG CTG CAG GTC GAC	*pYM44*		
		kt2073	TTCGCCGCTGCCCGCGGCAGCGCGGGCAGC TTTGTACAATTCATCCAT			
	DPM1	kt2081	TTGTACAAA GCTGCCCGCGCTGCCGCGGGCAGCGGCGAA ATGAGCATCGAATACTCTGT	gDNA YPH499		
		kt2082	TACCGGGCCCCCCCTCGAGGTCGAC TAATGATCTATTCATAAAGCA			
pRS415-GPDp-SCD6 FL	*SCD6*	kt2042	CGGCCGCTCTAGAACTAGTGGATCCATGTCGCAGTACATCGGTAAAAC	gDNA YPH499	*pRS415-GPDp*	*Bam*HI/*Xho*I
		kt2043C	ATTGGGTACCGGGCCCCCCCTCGAGTTAAAATTCAACGTTGGAAGGAGG			
pRS415-GPDp-SCD6 ΔRGG	*SCD6 ΔRGG*	kt2042	CGGCCGCTCTAGAACTAGTGGATCCATGTCGCAGTACATCGGTAAAAC	gDNA YPH499	*pRS415-GPDp*	*Bam*HI/*Xho*I
		kt2043A	ATTGGGTACCGGGCCCCCCCTCGAGTTAAGAGTGAAATCTTGGTCTGG			
pRS415-GPDp-SCD6 DLSm	*SCD6 ΔLSm*	kt2043B	CGGCCGCTCTAGAACTAGTGGATCCATGAATGACATACAGCCGGTTGTT	gDNA YPH499	*pRS415-GPDp*	*Bam*HI/*Xho*I
		kt2043C	ATTGGGTACCGGGCCCCCCCTCGAGTTAAAATTCAACGTTGGAAGGAGG			
pRS415-GPDp-SCD6 ΔFDF	*SCD6 LSm*	kt2042	CGGCCGCTCTAGAACTAGTGGATCCATGTCGCAGTACATCGGTAAAAC	gDNA YPH499	*pRS415-GPDp*	*Bam*HI/*Xho*I
		kt2043E1	AGAGTGAAATCTTGGTCTGGCGATGTTAGCATCTAAAATGCT			
	SCD6 RGG	kt2043E2	AGCATTTTAGATGCTAACATC GCCAGACCAAGATTTCACTCT	gDNA YPH499		
		kt2043C	ATTGGGTACCGGGCCCCCCCTCGAGTTAAAATTCAACGTTGGAAGGAGG			
pRS415-GPDp-EDC3 FL	*EDC3 FL*	kt2055N	CGGCCGCTCTAGAACTAGT ATGTCACAATTTGTTGGTTTC	gDNA YPH499	*pRS415-GPDp*	*Spe*I/*Xho*I
		kt2056	TACCGGGCCCCCCCTCGAG TTACAAATCTAATAGCAGGG			
pRS415-GPDp-EDC3 ΔYjeF_N	*EDC3 ΔYjeF_N*	kt2055N	CGGCCGCTCTAGAACTAGT ATGTCACAATTTGTTGGTTTC	gDNA YPH499	*pRS415-GPDp*	*Spe*I/*Xho*I
		kt2057	TACCGGGCCCCCCCTCGAG TTATAGTAGTTGTACTGGTGT			
pRS415-GPDp-EDC3 ΔLSm	*EDC3 ΔLSm*	kt2097c	CGGCCGCTCTAGAACTAGTGGATCC ATG GAACATATTGATTGGCAA	gDNA YPH499	*pRS415-GPDp*	*Spe*I/*Xho*I
		kt2056	TACCGGGCCCCCCCTCGAG TTACAAATCTAATAGCAGGG			

Table S2 (continued)

pRS415-GPDp-EDC3 ΔFDF-YjeF_N	*EDC3 LSm*	kt2087	CGGCCGCTCTAGAACTAGTGGATCC ATGTCACAATTTGTTGGTTTCG	gDNA YPH499	*pRS415-GPDp*	*Bam*HI/*Xho*I
		kt2097a	TACCGGGCCCCCCCTCGAGGTCGAC TTA ACCGCGATTTTGATTATAATC			
pRS415-DHH1p-EDC3(aa 1-86)-mCherry	*DHH1p*	kt2094	AGGGAACAAAAGCTGGAGCTC TGGTGTTGCAATATTGGACAA	gDNA YPH499	*pRS415-TEFp*	*Sac*I/*Sal*I
		kt2095	GAAACCAACAAATTGTGACATTACTACTATTTTCTTTCTTGT			
	EDC3(aa 1-86)	kt2096	ACAAGAAAGAAAATAGTAGTA ATGTCACAATTTGTTGGTTTC	gDNA YPH499		
		kt2097b	GTCGACCTGCAGCGTACG ACCGCGATTTTGATTATAATC			
	mCherry	kt2103	CGT ACG CTG CAG GTC GAC	*pYM-mCherry-kanMX*		
		kt2070a	TACCGGGCCCCCCCCTCGAGGTCGAC ATGGGGATGTATGGGCTAAA			
pRS415-DHH1p-DHH1-mCherry	*DHH1p-DHH1*	kt2079	AGGGAACAAAAGCTGGAGCTC TTTTCTTATCATTAGTGTCGC	gDNA YPH499	*pRS415-TEFp*	*Sac*I/*Sal*I
		kt2100	GTCGACCTGCAGCGTACG ATACTGGGGTTGTGACTGACC			
	mCherry	kt2103	CGT ACG CTG CAG GTC GAC	*pYM-mCherry-kanMX*		
		kt2070a	TACCGGGCCCCCCCCTCGAGGTCGAC ATGGGGATGTATGGGCTAAA			
pRS415-DHH1p-EDC3(1-86)-DHH1-mCherry	*DHH1p*	kt2094	AGGGAACAAAAGCTGGAGCTC TGGTGTTGCAATATTGGACAA	gDNA YPH499	*pRS415-TEFp*	*Sac*I/*Sal*I
		kt2095	GAAACCAACAAATTGTGACATTACTACTATTTTCTTTCTTGT			
	EDC3(aa 1-86)	kt2096	ACAAGAAAGAAAATAGTAGTA ATGTCACAATTTGTTGGTTTC	gDNA YPH499		
		kt2097	TTCGCCGCTGCCCGCGGCAGCGCGGGCAGC ACCGCGATTTTGATTATAATC			
	DHH1	kt2098	GCTGCCCGCGCTGCCGCGGGCAGCGGCGAA ATGGGTTCCATCAATAATAACTTC	gDNA YPH499		
		kt2100	GTCGACCTGCAGCGTACG ATACTGGGGTTGTGACTGACC			
	mCherry	kt2103	CGT ACG CTG CAG GTC GAC	*pYM-mCherry-kanMX*		
		kt2070a	TACCGGGCCCCCCCCTCGAGGTCGAC ATGGGGATGTATGGGCTAAA			
pRS415-DCP2p-DCP2-GFP	*DCP2p-DCP2*	kt2072	AGGGAACAAAAGCTGGAGCTC ATAATAAGGGTCATCGATCC	gDNA YPH499	*pRS415-TEFp*	*Sac*I/*Sal*I
		kt2068	GTCGACCTGCAGCGTACGCTTCCTATGCAAAATGCTTAA			
	GFP	kt2069	TTAAGCATTTTGCATAGGAAG CGT ACG CTG CAG GTC GAC	*pYM44*		
		kt2070a	TACCGGGCCCCCCCCTCGAGGTCGACATGGGGATGTATGGGCTAAA			
pRS415-DCP2p-DCP2-GFP NLS R229	*DCP2p-DCP2-mut.1*	kt2072	AGGGAACAAAAGCTGGAGCTC ATAATAAGGGTCATCGATCC	*pRS415-DCP2p-DCP2-GFP*	*pRS415-TEFp*	*Sac*I/*Sal*I
		kt2142	CGTTAACCACATTGATAAGGGTGTCATCATGGAATTAATCAG			
	DCP2-mut. 2-GFP	kt2143	TTA TCA ATG TGG TTA ACG CAT CAG ACT CAA ATA AAA AAT GAA GAT			
		kt2070a	TACCGGGCCCCCCCCTCGAGGTCGACATGGGGATGTATGGGCTAAA			
pRS415-DCP2p-DCP2-GFP NLS K450	*DCP2p-DCP2-mut.1*	kt2072	AGGGAACAAAAGCTGGAGCTC ATAATAAGGGTCATCGATCC	*pRS415-DCP2p-DCP2-GFP*	*pRS415-TEFp*	*Sac*I/*Sal*I
		kt2138	TGTAAGCGTTGGCGTTGTGCTTGATTGCACGTTGCTGTC			
	DCP2-mut. 2-GFP	kt2139	ACA ACG CCA ACG CTT ACA ATC TTA CAG AGA GGA ACG GAC			
		kt2070a	TACCGGGCCCCCCCCTCGAGGTCGACATGGGGATGTATGGGCTAAA			
pRS415-DCP2p-DCP2-GFP NLS S564+K697	*DCP2p-DCP2-mut.1*	kt2072	AGGGAACAAAAGCTGGAGCTC ATAATAAGGGTCATCGATCC	*pRS415-DCP2p-DCP2-GFP*	*pRS415-TEFp*	*Sac*I/*Sal*I
		kt2136	TGGTGTTTCCGTTTGACTTGTTGTGCTGTCTTTTTCGCTTGGCAT			
	DCP2-mut. 2-GFP	kt2137	ACA AGT CAA ACG GAA ACA CCA ACG AAC GAC GCA AGC AAA ACA AAC			
		kt2134	TAGTATTGTAACTGTGGGTACCGTTGTTACAGTATTTGTTGTTGATGA			
	DCP2-mut. 3-GFP	kt2135	GTA CCC ACA GTT ACA ATA CTA ACA ACA GGT GAA ACC TTT GCC AGT CTG			
		kt2070a	TACCGGGCCCCCCCCTCGAGGTCGACATGGGGATGTATGGGCTAAA			

Table S2 (continued)

pRS415-DCP2p-DCP2-GFP NLS R229+K450	*DCP2p-DCP2-mut.1*	kt2072	AGGGAACAAAAGCTGGAGCTC ATAATAAGGGTCATCGATCC	*pRS415-DCP2p-DCP2-GFP NLS K450*	*pRS415-TEFp*	*Sac*I/*Sal*I
		kt2142	CGTTAACCACATTGATAAGGGTGTCATCATGGAATTAATCAG			
	DCP2-mut. 2-GFP	kt2143	TTA TCA ATG TGG TTA ACG CAT CAG ACT CAA ATA AAA AAT GAA GAT			
		kt2070a	TACCGGGCCCCCCCTCGAGGTCGACATGGGGATGTATGGGCTAAA			
pRS415-NLS-3xGFP	*5'-NLS-GFP*	kt2144	TCTAGAACTAGTGGATCC ATG CCA AAG AAG AAA AGA AAG GTT CGT ACG CTG CAG GTC GAC	*pYM44*	*pRS415-GPDp*	*Bam*HI/*Xho*I
		kt2073	TTCGCCGCTGCCCGCGGCAGCGCGGGCAGC TTTGTACAATTCATCCAT			
	middle GFP	kt2147	GCTGCCCGCGCTGCCGCGGGCAGCGGCGAA CGT ACG CTG CAG GTC GAC			
		kt2148	CTCTCCAGATCCAGCTGCGGCCCGCGCGGC TTTGTACAATTCATCCAT			
	GFP-3'	kt2149	GCCGCGCGGGCCGCAGCTGGATCTGGAGAG CGT ACG CTG CAG GTC GAC			
		kt2070	GGTACCGGGCCCCCCCTCGAG ATGGGGATGTATGGGCTAAA			
pRS415-EDC3p-EDC3^{LSm}-GFP-DPM1	*EDC3p-EDC3 LSm*	kt2086	AGGGAACAAAAGCTGGAGCTC TAAAAAATGTCGTGATATTGC	gDNA YPH499	*pRS415-TEFp*	*Sac*I/*Sal*I
		2097b	GTCGACCTGCAGCGTACG ACCGCGATTTTGATTATAATC			
	GFP-DPM1	kt2082	TACCGGGCCCCCCCTCGAGGTCGAC TAATGATCTATTCATAAAGCA	*pRS414-DCP2p-DCP2-GFP-DPM1*		
		kt2103	CGT ACG CTG CAG GTC GAC			
pRS415-EDC3p-EDC3$^{LSm\text{-}FDF}$-GFP-DPM1	*EDC3p-EDC3 LSm-FDF*	kt2086	AGGGAACAAAAGCTGGAGCTC TAAAAAATGTCGTGATATTGC	gDNA YPH499	*pRS415-TEFp*	*Sac*I/*Sal*I
		kt2146	GTCGACCTGCAGCGTACG TAGTAGTTGTACTGGTGT			
	GFP-DPM1	kt2082	TACCGGGCCCCCCCTCGAGGTCGAC TAATGATCTATTCATAAAGCA	*pRS414-DCP2p-DCP2-GFP-DPM1*		
		kt2103	CGT ACG CTG CAG GTC GAC			
pRS415-SCD6p-SCD6^{LSm}-GFP-DPM1	*SCD6p-SCD6 LSm*	kt2127	AGGGAACAAAAGCTGGAGCTC AGACTCTAGAGTTAACATTGA	gDNA YPH499	*pRS415-TEFp*	*Sac*I/*Sal*I
		kt2130	GTCGACCTGCAGCGTACG GATGTTAGCATCTAAAATGC			
	GFP-DPM1	kt2082	TACCGGGCCCCCCCTCGAGGTCGAC TAATGATCTATTCATAAAGCA	*pRS414-DCP2p-DCP2-GFP-DPM1*		
		kt2103	CGT ACG CTG CAG GTC GAC			
pRS415-SCD6p-SCD6$^{LSm\text{-}FDF}$-GFP-DPM1	*SCD6p-SCD6 LSm-FDF*	kt2127	AGGGAACAAAAGCTGGAGCTC AGACTCTAGAGTTAACATTGA	gDNA YPH499	*pRS415-TEFp*	*Sac*I/*Sal*I
		kt2145	GTCGACCTGCAGCGTACG AGAGTGAAATCTTGGTCTGG			
	GFP-DPM1	kt2082	TACCGGGCCCCCCCTCGAGGTCGAC TAATGATCTATTCATAAAGCA	*pRS414-DCP2p-DCP2-GFP-DPM1*		
		kt2103	CGT ACG CTG CAG GTC GAC			

Table S3. qPCR Primers used in the study

Target	Primer name	Primer sequence	Reference
ACT1	CW961	AGGTTGCTGCTTTGGTTATTG	Wang *et al.* (2018)
	CW962	CCGACGATAGATGGGAAGAC	
BSC1	CW562	TCTGACGGTTGCACAGTTTG	
	CW729	TGCCAAGTTTGCCAGTACTG	
EDC3^{LSm}	ktq037	ATGGGAAGCTCATTCAGGGG	This study
	ktq038	CACCATCGCCGAATTGAACG	
EDC3$^{FDF\text{-}YjeF\_N}$	ktq039	AACTCGGCAGGGCTACTAGA	
	ktq040	CGGCCACCTAGTTTCTGCTT	
ILM1	CW969	CAATTGGGTCTTTTCGCTCT	Wang *et al.* (2018)
	CW970	CTGGCACAACAGATTGGAAG	
PGK1	CW963	TTGATTGACAACTTGTTGGA	
	CW964	CAGTGACAGTCTTGGTGTTG	
SCD6^{LSm}	ktq033	AGAAGGTCGCAAGAACTGGG	This study
	ktq034	TCCTTGACTTCACTGCCGTT	
SCD6^{RGG}	ktq035	CTCAAGCACACGTGCAAACA	
	ktq036	ACACCATATCCAGCGACAGC	

Supplementary References

Kilchert, C. (2010). mRNA localization and turnover in mutants of the small GTPase Arf1p of Saccharomyces cerevisiae. PhD thesis, University of Basel, Switzerland. http://edoc.unibas.ch/diss/DissB_9195

Sikorski, R. S. and Hieter, P. (1989). A system of shuttle vectors and yeast host strains designed for efficient manipulation of DNA in *Saccharomyces cerevisiae. Genetics* 122, 19-27. doi:10.1093/genetics/122.1.19